EVALUATION OF THE THERMAL PERFORMANCE OF WALLS USING TIME LAG AND DECREMENT FACTOR

BY

KOJO ADOM QUAGRAINE

A Thesis Submitted to

the Department of Mechanical Engineering

Kwame Nkrumah University of Science and Technology, Kumasi, Ghana

In partial fulfillment of the requirements for the

Degree of

MASTER OF PHILOSOPHY IN MECHANICAL ENGINEERING

April, 2019

DECLARATION

I hereby declare that this submission is my own work and that, to the best of my knowledge and belief, it contains no material previously published or written by another person nor material which to a substantial extent has been accepted for the award of any other degree or diploma at Kwame Nkrumah University of Science and Technology, Kumasi or any other educational institution, except where due acknowledgement is made in the thesis.

Quagraine Kojo Adom	……	……..
Candidate	Signature	Date

CERTIFICATION

Dr. Emmanuel Ramde	……	……..
(Supervisor)	Signature	Date

Professor G.Y. Obeng	……	……..
(Head of Department)	Signature	Date

DEDICATION

This work is dedicated to God and my family.

ACKNOWLEDGEMENT

I would like to express gratitude to my supervisor Dr. E. W. Ramde for his constructive criticisms, suggestions and guidance which has helped in producing this work.

I wish to also express gratitude to my family members for the help, encouragement, support and prayers. A special thanks goes to my parents Mr. Francis Eku Quagraine and Mrs. Rose Elizabeth Quagraine; my sisters Araba Quagraine and Ethel Quagraine.

I am grateful to be in the midst of supportive course mates during my postgraduate studies.

I would also like to thank Mr. Joseph Nyumutsu and Mr. Joseph Gadossey.

Finally I thank the Almighty God for His blessings, help and guidance.

ABSTRACT

This study dealt with the evaluation of the thermal performance of walls in the climatic area of Kumasi using the parameters time lag and decrement factor. A numerical model was developed using the finite volume method with implicit formulation for four different wall configurations used in building constructions in Kumasi. The wall configurations had the same thickness and consisted of the mass concrete block wall, hollow concrete wall, mud brick wall and sandrete block wall. The simulation was carried in the month of March and August which respectively have the highest and lowest global solar radiation and dry bulb air temperature using mathcad software tool. The results showed that the heat gain by the walls through irradiation and ambient temperature in the area had some impact on the time lag and the decrement factor of the wall. The time lag values for the hollow concrete wall, mud wall and sandcrete had high values in March when the level of global solar radiation and outside dry bub temperature was high and reduced by an hour in August when the levels were low. The highest time lag was achieved by the mud brick wall which had five hours in the month of March. This was followed by the mass concrete wall which had time lag value of four hours for both months. The lowest decrement factor value was also given by the mud brick wall in the month of March whiles the lowest decrement factor in the month of August was given by the sandcrete block wall which also followed the mud brick wall closely in March. The numerical model was verified with analytical solution. The study is important in determining heat storage capabilities and temperature fluctuation reduction in wall configurations used in the West African tropical savannah climatic area.

TABLE OF CONTENT

LIST OF TABLES

Table No. Title Page

LIST OF FIGURES

Figure No. Caption Page

LIST OF ABBREVIATIONS

hrs	-	Hours
KNUST	-	Kwame Nkrumah University of Science and Technology
kWh	-	Kilowatts hour
W/m^2K	-	Watts per meter squared Kelvin
km/h	-	Kilometer per hour
mm	-	Millimeters
RMSE	-	Root Mean Square Error
MPE	-	Mean Percentage Error
MBE	-	Mean Bias Error

NOMENCLATURE

a	-	Absorptance of surface for solar radiation
α	-	Thermal diffusivity of the wall material
c	-	Specific heat (J/kg K)
ρ	-	Density of the material (Kg/m^2)
ε	-	Emissivity of the inner surface of wall
E_t	-	Global solar radiation on surface, W/m^2
F_o	-	Dimensionless mesh Fourier number
h_c	-	Convective heat transfer of the room (W/m^2K)
h_o	-	Outside heat transfer coefficient (W/m^2K)
k	-	Thermal conductivity of the material $(W/m K)$
q_g	-	Heat generation of the material
t_{out}	-	Outside dry bulb air temperature (˚C)
t_{wo}	-	Outer surface temperature of wall (˚C)
t_{wi}	-	Indoor surface temperature (˚C)
t_i	-	Indoor air temperature (˚C)
$t_{Tin\ max}$	-	Inside surface maximum temperature of the wall (˚C)
$t_{Tout\ max}$	-	Outside surface maximum temperatures of the wall (˚C)
$T_{in\ (max)}$	-	Maximum inside surface temperature (˚C)
$T_{in\ (min)}$	-	Minimum inside surface temperature (˚C)
$T_{out\ (max)}$	-	Maximum outside surface temperature (˚C)
out (min)	-	Minimum outside surface temperature (˚C)

T

G_{pred} - Predicted temperature Value

G_{anal} - Analytical temperature Value

CHAPTER ONE

1.0 INTRODUCTION

1.1 Background

Building with energy conservation is an important factor as heating, ventilating, and air conditioning systems consume large amount of energy in the society. A good method to lower the building consumption is to design building configurations that are energy saving. Natural air conditioning effect (cooling or warming when necessary) can be achieved by some specified building envelope configuration (Sun et al., 2013).

Building envelope comprises a configuration with different thermo-physical properties and materials which determine how the envelope responds to climatic conditions. The prevalent environmental conditions also determine the building's climatic response. The material configuration of the building geometry and its properties have the ability to thermo-regulate and enhance thermal comfort in the building (Balaji et al., 2013).

In general, the heat transfer to building envelopes is unsteady due to the variations of solar radiation and temperature throughout the day. The thermal capacity of the wall brings about unequal heat flow between the outer surface and the inner surface due to unsteady conditions at an instant.

The heat flow through the walls determines the cooling/heating load in the room. This means that the thermal comfort and the energy consumption of the building are influenced by the thermal performance of the wall because the variations of the indoor temperature in the room are caused by the heat flow through the wall. Researchers reduce the energy consumption of building configurations and enhance the thermal comfort of the wall by developing efficient walls (Jin et al., 2012).

Passive cooling and heating through solar radiation is an effective application of solar energy in buildings. In this application, the energy from solar radiation is stored in the building through the walls and floors during the day and is used for heating during the night. Enhancing thermal comfort and minimising building energy consumption can be achieved through natural and passive heating and cooling systems (Fathipour and Hadidi, 2017). Heat gain is made up of components which affect cooling load like conduction through walls, windows and roofs; heat transmission from the outside air through openings; heat from equipment and people in the building (Oktay et al., 2016).

In transient thermal analysis, thermal resistance and thermal inertia are important in the analysis of walls. The exterior wall acts like a capacitor throughout the day and night by absorbing heat during the day and rejecting it in the night. A thermal heat wave propagates from the outside of the building to the inside of the building due to temperature fluctuations outside the building. The heat waves amplitude reduces due the material properties and thickness of the wall (Asan and Sancaktar, 1998; Rosti and Omidvar, 2013).

The heat gain in the room, conduction and radiation at the face of the building varies with time; hence the thermal behaviour of the wall can be predicted using a transient model. When the heat wave propagates through the wall, the attenuation of its amplitude depends on the thickness and the material properties of the layers of the wall. The time period required for the heat wave to propagate from the outer surface to the inner surface of the wall is called the time lag. The ratio of the heat wave amplitudes at the two surfaces of the wall is referred as the decrement factor. The heat flow from the inner surface is less than the heat flow into the outer surface due to the thermal capacity of the wall and this is taken into account by the decrement factor. The time lag and decrement factor are important parameters in evaluating the thermal performance of walls because they determine its heat storage abilities (Asan,

2006; Ruivo et al., 2013).

1.2 Problem Statement

The energy consumption of buildings is continuously becoming a concern given the energy demand in Ghana. Building envelopes and renovated buildings employ inadequate energy efficient designs in building envelopes. Due to increasing energy consumption in buildings, it is important to use building envelope configurations which reduce the energy consumption in buildings.

The energy consumption in buildings and the thermal comfort of the room is influenced by the thermal performance of the wall. Maintaining a stable temperature indoor is a key aspect of thermal comfort. In conditions where the outside temperature fluctuates widely it is desirable to keep the indoor temperature constant. There are two parameters which can evaluate the thermal performance of walls. They are the time lag and decrement factor. These parameters are important in the design of energy efficient building envelope configurations in Ghana. They also determine the heat storage capabilities of buildings.

1.3 Aim of study

The main objective of the study is to evaluate the thermal performance of different configuration of walls in Kumasi using the parameters time lag and decrement factor.

1.4 Specific Objectives

The specific objectives are:

- To determine the time lag and decrement factor of the different building wall configurations in Kumasi.
- To determine the temperature variations across the thickness of wall configurations in Kumasi.
- To determine the impact of climatic data of the month on time lag and decrement factor of building envelopes in Kumasi.
- To determine the temperature variations at the inner and outer surfaces of the wall.

1.5 Justification

An energy efficient building improves the energy savings in a building. Developing countries employ traditional solutions like putting up heavy mass buildings which are no longer economical due to increasing land costs and shortage of building materials. In addition, many passive solar building designs just utilize high insulation levels (Lakatos, 2017).

The time lag and decrement factor are important parameters of materials and building envelopes. The delay in time in heat flow between the inside and outside surface caused by the thermal mass is called the time lag. The reducing ratio of the cyclical temperature from the inside surface to the outside surface is known as the decrement factor.

In hot tropical climates, these parameters are important in designing energy efficient buildings. The constantly hot temperatures can cause the thermal mass effect to be detrimental. The reason is that average daily temperature at both surfaces can approach the same value which if it is below or above the thermal comfort of the room can lead to uncomfortable conditions due to unwanted heat gain or loss.

The knowledge about the parameters time lag and decrement factor of building envelopes in Ghana will help select energy efficient building envelopes which will reduce the cooling capacity of building envelopes. This will make it possible to maintain thermally comfortable temperatures in the building envelope. In addition, it will also reduce the use of air conditioning system in buildings which will improve the energy consumption of the building envelope.

1.6 Structure of the Thesis

This thesis is structured into five chapters which consist of introduction, literature review, methodology, conclusions and recommendation. Chapter One contains the introduction which discusses the background to the research topic, problem statement, main objective of the thesis and the specific objectives and finally the scope of work and organization of thesis. Chapter Two reviews existing literatures on relevant areas relating to this study which provides an

insight into research done by previous works and a theoretical framework for this thesis. Chapter Three explains the methodology used to undertake this research and consists of the model used in the simulation and the validation process employed. Chapter Four discusses the results obtained from the simulations. The final chapter concludes the thesis by giving a summary of the major findings and makes recommendations from the research.

CHAPTER TWO

2.0 CLIMATIC RESPONSE OF TIME LAG AND DECREMENT FACTOR FOR BUILDING MATERIALS

2.1 Chapter outline

This literature review examines literatures on the general climate of Kumasi, building materials used in the city, the thermal properties of buildings and its relationship with thermal performance, and also passive solar energy and its applications in buildings. This chapter finally ends with a review of papers published on the parameters time lag and decrement factor.

2.2 General climate of Kumasi

Ashanti region has thirty districts including Kumasi Metropolis. It is located in South Central Ghana at a distance of 270 km north of the nation's capital. Kumasi Metropolis has a location between latitude 6.35 ˚N and 6.40 ˚N and also longitude 1.30 ˚W and 1.35 ˚W. It has an elevation of 250 to 300 meters above sea level with 214.3 square kilometres surface area. Kumasi Metropolis has an average minimum temperature of 21.5 degrees centigrade and an average maximum temperature of 30.7 degrees centigrade whiles the average humidity at sunset is 60 percent and at sunrise is about 84.16 percent (Ghana Statistical Service, 2014). Kumasi Metropolis is in the moist semi-deciduous south-east ecological zone of the country with exotic species as the most common tree genera. The climate is tropical with a bi-modal rainfall system which has a major rainfall season from April to June and a minor rainfall season from September to October. The mean annual rainfall is 1250 mm (Nero et al., 2017). The two rainfall seasons which occur within the year are part of the wet season. The harmattan period which occurs between December and January carries dust due to dry winds blowing southwards across the Sahara desert. The dust raises the turbidity of the atmosphere and increases solar radiation dispersion (Moujaled, 2014).

2.3 Building materials used in Kumasi

The construction materials used for the outer walls in Kumasi metropolis depends on their cost and availability. The Ghana statistical service administered questionnaires and found that 90.5 per cent of material for the outer walls of dwelling units in Kumasi metropolis is made of mass concrete blocks. The concrete blocks also has a higher percentage in the region and in the country with values of 71.9 per cent and 57.5 respectively. However, timber and mud brick have 3.3 percent and 2.8 percent respectively. The main construction material for outer wall of dwelling units by type of locality is shown in Table 2.1.

Table 2.1: Main construction material for outer wall of dwelling units by type of locality

	TOTAL COUNTRY		ASHANTI REGION		KUMASI METROPOLIS		
Material Outer wall	**Number**	**Percent**	**Number**	**Percent**	**Number**	**Percent**	**Urban**
Mud brick/earth	1,991,540	34.2	250,238	21.4	12,635	2.8	2.8
Wood	200,594	3.4	27,438	2.3	14,577	3.3	3.3
Metal sheet/slate	43,708	0.8	10,549	0.9	4,920	1.1	1.1
Stone	11,330	0.2	2,014	0.2	730	0.2	0.2
Burnt bricks	38,237	0.7	7,580	0.6	1,939	0.4	0.4
Concrete block	3,342,462	57.5	840,519	71.9	404,219	90.4	90.4
Sandcrete	104,270	1.8	19,878	1.7	2,382	0.5	0.5
Bamboo	8,206	0.1	1,381	0.1	490	0.1	0.1
Palm leaf/ thatch	38,054	0.7	1,768	0.2	345	0.1	0.1
Others	39,206	0.7	7,665	0.7	4734	1.1	1.1
Total	5,817,607	100	1,169,030	100	446,971	100	100

SOURCE: Ghana Statistical Service, 2014.

2.4 Thermal properties of building materials

The thermal properties of buildings are important in the thermal performance of buildings. The thermal properties of buildings include the thermal conductivity, thermal diffusivity, thermal mass, thermal inertia and thermal diffusivity.

Long and Ye (2015) investigated the effect of thermo-physical properties on the thermal performance of walls in Hefei, China. The results show that, thermo-physical properties such as thermal conductivity and heat capacity of the building have influence on the energy performance of the building. The study also concluded that for better thermal performance in Hefei, China the thermal conductivity should be low and the heat capacity of the material should be high.

The thermal conductivity of a material is defined by Kumar (2009) as "the rate of heat transfer through a unit thickness of a material per unit temperature difference per unit area perpendicular to the direction of heat flow." Thermal conductivity is a property of a material which depends on its chemical and physical structure, moisture content, density, and the operating conditions of temperature and pressure. The thermal conductivity of material ranges between the values of 0.0083 W/m K for gases like Freon-12 to bigger values like 410 W/m K for metals such as silver (Kumar, 2009).

The thermal mass determines the ability to store heat as latent or sensible heat which influences indoor temperature and thermal comfort (Reilly and Kinnane, 2017). When considering the heat capabilities of buildings; the two thermal properties considered are the heat absorption rate and the heat capacity by volume. The heat absorption rate determines the ability of the element to conduct thermal energy. The heat capacity determines the ability of the element to store thermal energy (Li and Xu, 2006).

The thermal inertia is a term used to describe the effect of thermal mass on the thermal behaviour of buildings. It lacks a uniform definition in literature (Verbeke and Audenaert, 2018). Merriam Webster online dictionary defines thermal inertia as the degree of slowness in which the environment and the body approach the same temperature and it is dependent upon the body's thermal conductivity, specific heat, absorptivity, its dimensions and other factors.

This term is similar to motion inertia concept which is defined as "resistance of change in motion of an object". In earth science, it is defined as the “resistance to temperature change during a full heating/cooling cycle indicated by time dependent temperature variations (Verbeke and Audenaert, 2018).

The thermal diffusivity determines the ability of a material to conduct heat relative to the material’s ability to store thermal energy. Materials with high thermal diffusivity have a quick response to changes in the thermal environment whiles slow response to changes in thermal environment is associated with materials which have a low thermal diffusivity which takes longer periods to reach new equilibrium conditions (Incropera and DeWitt, 1990). A high thermal conductivity or low heat capacity value will give a high thermal diffusivity and vice versa. Thermal diffusivity shows how fast heat diffuses through a material.

2.5 Passive solar design

Passive solar design is resourceful way of heating and cooling buildings using building design configurations. This is performed using heat transfer modes like radiation, convection and conduction using solar energy as an advantage. Passive heating systems are categorized as either direct gain, indirect gain or isolated gain (Barber, 2012).

Direct gain is an application of passive solar energy where heat is received by the building directly through solar radiation. It is commonly used in the cold climates for cheap, simple and effective heating through thermal storage mass. For indirect gain, heat is transferred from the wall to the living space through air movement from the internal space. Solar heat gain in this application is through vents integrated into thermal mass which circulates air and distributes heat. Isolated heat gain uses natural or forced convection to cause heat to flow into the actual living space by using solar collection and thermal storage materials that is in a separate location from the actual living space. The basic composition of isolated heat gain is a collector which absorbs solar radiation to heat a fluid, a storage mass which absorbs and stores heat from the

fluid and finally a mechanism to distribute heat stored. Figure 2.1 shows the direct and isolated gain passive solar energy (Barber, 2012)

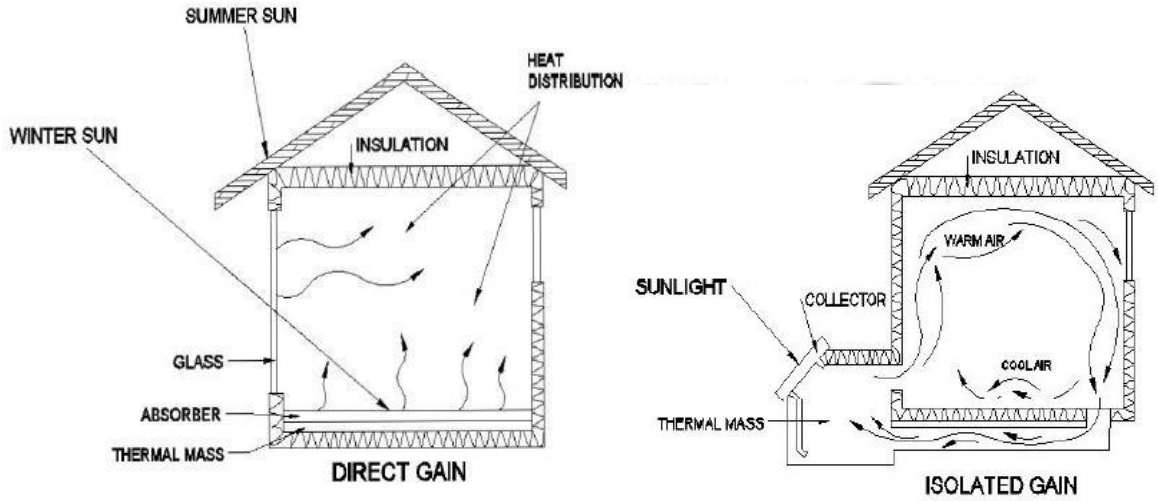

Figure 2.1: Direct and Isolated gain passive solar energy

SOURCE**:** Barber, 2012

Rodriguez-ubinas et al. (2014) analyzed the use of passive strategies and their influence in the buildings. A significant reduction of energy consumption of the building by passive solar strategies is plausible. The solar Decathlon Europe (SDE), an international competition about sustainable and high efficiency promoted education on the importance of passive strategies to people. Rodriguez-ubinas et al. (2014) also researched about solar Decathlon Europe (SDE) houses which included the strategies used and its effect on the thermal behaviour of the houses. A balance between envelope, orientation, geometric aspects and other passive strategies were achieved. The strategies reduced energy consumption of building and improved the hygrothermal comfort of the building.

Passive solar design strategies use energy from the sun to enhance thermal comfort in buildings without the use of Mechanical or electrical equipment. The key passive solar design factor is to take advantage of the climate of the surroundings. Heat storage is an important technique in reducing energy usage in buildings. The advantages of heat storage in buildings are that it reduces the peak power in heating and cooling buildings. It shifts peak heating and cooling

loads to low tariff hours and also shifts temperature peaks to non-working hours. Furthermore there is improvement in indoor environment and passive heating and cooling loads are efficiently utilized (Velraj and Daniel, 2014).

2.6 Time lag and decrement factor

Time lag or phase lag is the time it takes for a heat wave to move from the outer surface of the wall to the inner surface of that same wall. Decrement factor or attenuation factor is the decreasing ratio of the heat wave's amplitude (Asan, 2006). The time lag and decrement factor are important parameters in evaluating the thermal storage capabilities of materials (Asan and Sancaktar, 1998). The schematic diagram of time lag and decrement factor is shown in Figure 2.2.

When considering wall configurations with different layers, the arrangement of the layers of materials in which heat passes through is also a factor in determining the time lag and decrement factor. This implies that the control of time lag makes it possible to control and prevent the overheating of buildings (Balaji et al., 2013).

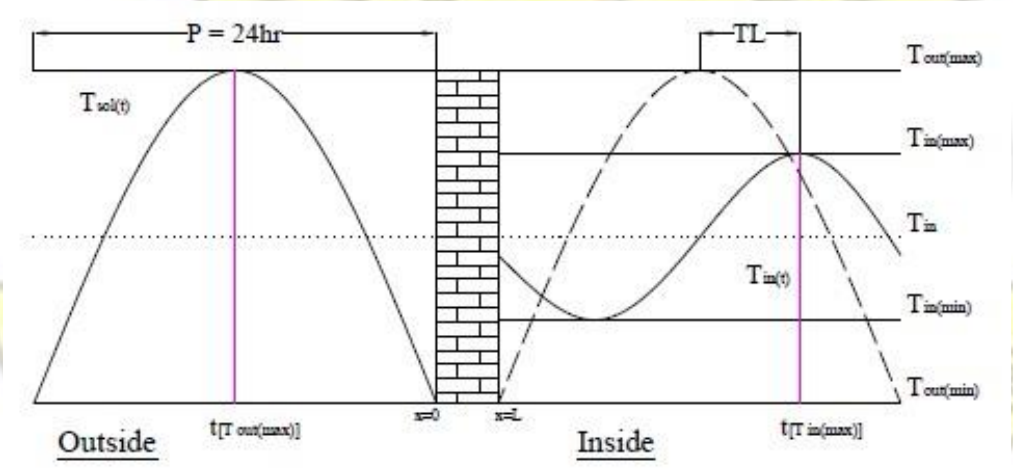

Figure 2.2: Schematic diagram of time lag and decrement factor
SOURCE: (Balaji et al., 2013)

Thermal comfort is associated with a stable indoor temperature. In conditions where the outside temperature fluctuates about a minimum and maximum outside temperature, it is desirable to maintain a constant indoor temperature. The configuration of the building envelope has the

ability to effectively dampen the degree of oscillation of temperature inside a building. “The decrement factor of the building configuration attenuates the amplitude of the outside temperature to that of the inside”. When the decrement factor tends to zero, the construction element has a great effect on the attenuation. This means that the smaller the decrement factor the more effective suppression of oscillations by wall (“GreenSpec:

Decrement Delay / Factor in the Building Envelope Fabric,” 2017).

Oktay et al. (2016) found that meteorological data of a particular area, solar absorptivity of the materials surface, and the thermo-physical properties of the materials have significant effect on time lag and decrement values. The study concluded that there is a relation between the selected wall material’s thermal conductivity and its decrement factor but it is difficult to establish a relation between the time lag of the selected wall material and its thermal conductivity.

Also, Faithpour and Hadidi (2017) developed an analytical solution to determine the time lag and decrement factors of buildings in Iran. The research asserted that the decrement factor and time lag changes with a changing combined convection and radiation heat transfer coefficients of the inner and outer environment. In addition, decrement factor decreases with increasing inside combined radiation and convection heat transfer coefficient.

Furthermore, Jin et al. (2012) defined the parameters heat flux time lag and heat flux decrement factor to analyze the flow of heat in a wall and also its influence on the thermal the properties. The thermal properties considered were thermal capacity and thermal conductivity. The research showed that heat flux time lag and heat flux decrement factor has influence on the thermal properties of wall. The heat flux time lag increases with the increase of thermal capacity but decreases with the increase of the thermal conductivity. However, the heat flux decrement factor increases with the increase of thermal conductivity but decreases with increase of the thermal capacity of the wall.

Ozel and Ozel (2012a) investigated the effect of wall orientation on three different wall insulation materials on the parameters time lag and decrement factor using the climatic data of Istanbul, Turkey. The study found that the wall orientation has a significant effect on time lag as maximum time lag values were obtain for east orientation but has a small effect on the decrement factor. In addition, Ozel and Ozel (2012b) in another paper conducted a study by comparing the thermal performance of six different wall configurations used in the climate of Izmir, Turkey facing the south orientation. The study showed that maximum temperature swings occurs in the concrete wall in the summer and winter months whiles minimum temperature swings occurs in the "ytong" wall for these same months.

In another research, Rosti and Omidvar (2013) performed transient thermal analysis on walls exposed to solar radiation and outside air temperature in the summer and winter months in the city of Tehran using its climatic conditions. The outside air temperature was assumed to be sinusoidal and fluctuated between the minimum and maximum temperature for the day and also for the year. Their results showed that decrement factor has no variation with the change in insulation location in the wall when the annual outside air temperature fluctuation is used but varies with change in insulation when the daily outside air temperature is employed.

However, Sun et al. (2013) studied the relationship between the outside temperature with time lag and decrement factor. The outside temperature wave was constructed with sinusoidal and non-sinusoidal periodic functions. The non-sinusoidal air temperature wave produces time lag crests unequal to time lag troughs. The time lag also varies with the increasing stage of the temperature wave whiles the decrement factor varies slightly with the temperature wave.

2.7 Chapter Summary

The Chapter reviews literature relevant to the study. The literature review is organized around the following topics:

i) general climate of Kumasi; ii) building materials used in Kumasi; iii) thermal properties of building materials; v) passive solar designs strategies; vi) time lag and decrement as parameters for evaluating thermal performance.

It was found that in previous literatures, there was limited research in the evaluation of thermal performance of walls in West African tropical savannah climatic areas using the parameters time lag and decrement factor. This study deals with the evaluation of the thermal performance of walls in Kumasi, Ghana (West African tropical savannah climatic area) using the parameters time lag and decrement factor.

CHAPTER THREE

3.0 METHODOLOGY

3.1 Chapter Outline

This chapter discusses the methodology used in the study. It begins with the mathematical model which shows the formulation of the sol air temperature and the finite difference equations used in the simulation. The wall composition and its thermo-physical properties which are the input parameters for the simulation are also presented in this chapter. The methodology concludes with the method of validating the mathematical model.

3.2 Mathematical model formulation

3.2.1 Sol air temperature

The sol-air temperature is the temperature which accounts for the effects of incident solar radiation changes and radiation energy exchange with the sky and other outdoor surroundings and convective heat exchange with the outside air.

The sol- air temperature equation is obtained from (ASHRAE, 2009) as;

$$\square \qquad \overline{a\ E^{+}} \quad \frac{\varepsilon \Delta R}{} \qquad 3.1$$

$t_{sol\ air} = t_{out} + \frac{a \cdot E_t}{h_o} - \frac{\varepsilon \Delta R}{h_o}$ ..... (3.1)

Where; a = Absorptivity of surface for solar radiation

E_t = Global solar radiation incident on surface, W/m²

h_o = Outside heat transfer coefficient (W/m^2K) t_{out} = Outside dry bulb air temperature (˚C)

The climatic data for Kumasi was obtained from the K.N.U.S.T solar laboratory. The data consisted of hourly outside dry bulb temperature, global radiation and wind speed for the month of August and March from the period between 2002 and 2004. The data was obtained in a spreadsheet format. It was averaged for the three years and was used as input parameters for the simulation.

The term ($\varepsilon \Delta R$) in the sol-air temperature equation was taken to be zero for vertical surfaces because long range radiation exchange between buildings was considered to be negligible.

The total global radiation incident on a vertical surface is given by Duffie and Beckman (2013) as;

$$E_T = I_b R + I_d \left(\frac{1+\cos\beta}{2}\right) + \rho \left(\frac{1-\cos\beta}{2}\right) \tau \times I_H \quad \text{..... 3.2}$$

Where,

β = tilt angle of wall, ˚ τ = Ground reflectance

I_H = Hourly total horizontal radiation, W/m²

I_b = Hourly total beam radiation, W/m²

I_d = Hourly total diffuse radiation, W/m²

$R_b = \frac{\cos\theta}{\eta \cos\theta_z}$; θ = Incidence angle; θ_z = zenith angle for any latitude, $\eta \cos\theta_z$

The outside heat transfer coefficient varies and is a function of wind speed. The empirical equation for the heat transfer coefficient is obtained from (Rohsenow et al., 1985) as;

$$h_o = 18.63\ V^{0.605} \quad \text{3.3}$$

Where;

$V = 0.25$ if $V \leq 2$ m/s

$V = 0.50$ if $V > 2$ m/s

The inside surface heat transfer coefficient for the wall is also obtained from (Rohsenow et al., 1985) as;

$$h_i = h_c + 5.72\varepsilon \quad \text{3.4}$$

Where; ε = emissivity of the inner surface of wall h_c =convective heat transfers of the room and is dependent on the direction of heat flow;

$h_c = 4.04$ *upward*

$h_c = 3.87$ 45 *upward*

$h_c = 3.08$ *horizontal*

$h_c = 2.28$ 45 *downward*

$h_c = 0.920$ *download*

The sol-air temperature was solved to get $T_{sol}^{max}{}_{\alpha air}$ and $T_{sol}^{min}{}_{\alpha air}$ which are the maximum and minimum sol-air temperatures. The sinusoidal sol –air temperature varies between the

maximum and minimum sol-air temperatures. The daily sinusoidal sol-air temperature is given by Ruivo et al. (2013) as;

$$T_{sol-air(t)} = \frac{T^{max}_{sol-air} + T^{min}_{sol-air}}{2} \sin\left(\frac{2\pi t}{P} - \frac{\pi}{2}\right) + \frac{T^{max}_{sol-air} - T^{min}_{sol-air}}{2} \qquad 3.5$$

3.2.2 Heat conduction equation

The general heat conduction which relates time and spatial variation of temperature is given as;

$$\frac{\delta}{\delta x}\left(k_x \frac{\delta T}{\delta x}\right) + \frac{\delta}{\delta y}\left(k_y \frac{\delta T}{\delta y}\right) + \frac{\delta}{\delta z}\left(k_z \frac{\delta T}{\delta z}\right) + q_g = \rho C \frac{\delta T}{\delta t} \qquad 3.6$$

Where; k = thermal conductivity of the material $(W/m \cdot K)$ T = Temperature of the material (˚C)

ρ = Density of the material (Kg/m^2)

C = specific heat of the material (J/kg K) q_g = heat generation of the material

The one dimensional transient heat conduction equation for constant thermal conductivity with no heat generation inside the multi-layered wall is given as;

$$k \frac{\delta^2 T}{\delta x^2} = \rho C \frac{\delta T}{\delta t} \qquad 3.7$$

Solving the partial differential equation above requires two boundary conditions and an initial condition. The convection boundary conditions at the inner and outer surfaces of the wall are a more comprehensive and complex type of boundary condition.

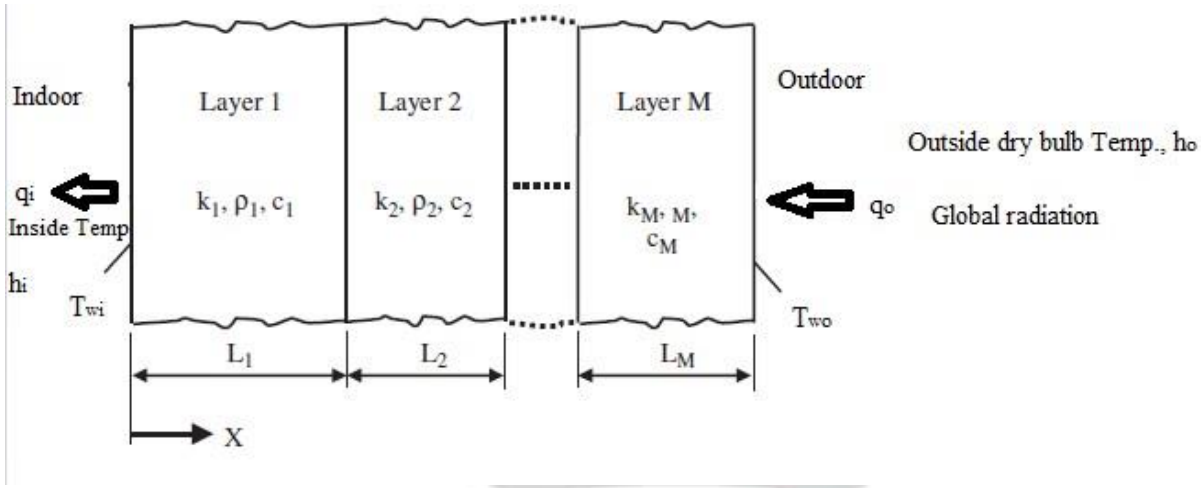

Figure 3.1: Heat conduction in a multilayer

The boundary condition at the outer surface of the wall in Figure 3.1 is given as;

$$k_m \frac{\partial T}{\partial x}_{x=L} = h_o (t_{sol\ air} - t_{wo}) \quad \text{3.8}$$

Where; t_{wo} = outer surface temperature of wall (˚C)

k_1= thermal conductivity at the first layer (W/mK)

The boundary condition at the inner surface of the wall is given as;

$$-k_1 \frac{\partial T}{\partial x}_{x=0} = h_i (t_{wi} - t_i) \quad \text{3.9}$$

Where; t_{wi} = indoor surface temperature (˚C) t_i =

indoor air temperature (˚C) k_m = thermal conductivity

at the mth layer $W/m K$

3.2.3 Finite difference formulation

A composite wall structure is shown with M-layers, boundary conditions at the outer and inner surfaces and grid arrangement in Figure 3.2.

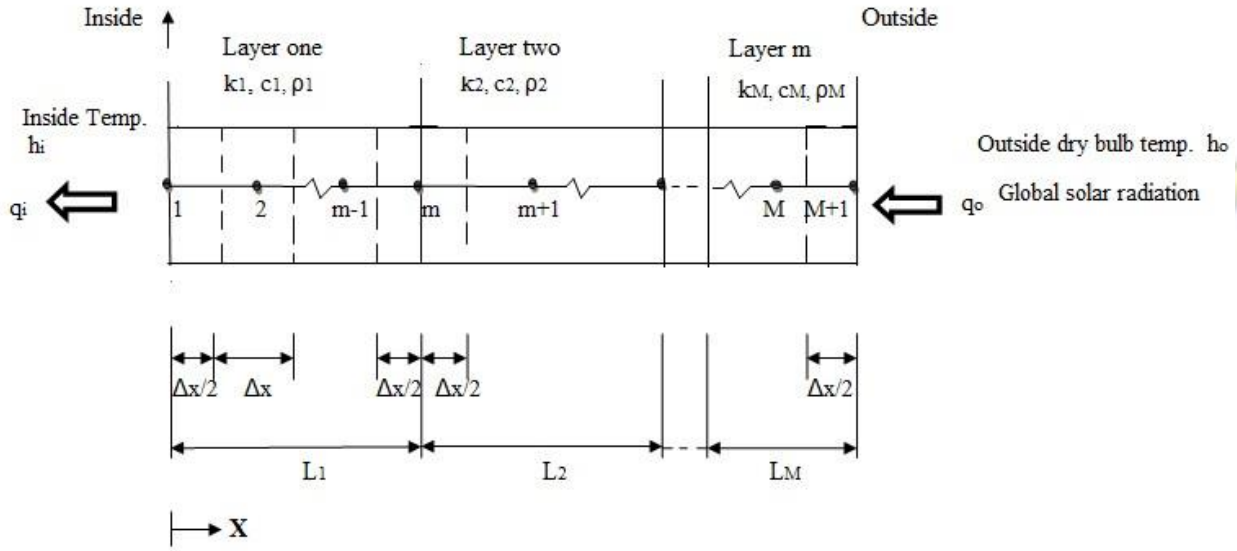

Figure 3.2: Node arrangement of a composite wall of M layers

The finite difference method for the nodes is obtained using energy balance on the element and is expressed as;

Heat transfered into Heat generated within The change in the
the volume element

□□□□fromduring all □ oft it's surfaces □□□□duringthe volume □t element □□□□□□□energy volumecontent during □oft the□□□

$$\Delta t \sum_{\text{Allsides}} Q \pm G_{element} \Delta t = \Delta E_{elemrnt} = \rho V_{element} C \left(T_{mp+1} - T_{mp} \right) \quad (3.10)$$

The equation 3.10 is expressed without heat generation as;

$$\Delta t \sum_{\text{Allsides}} Q = \Delta E_{elemrnt} = \rho V_{element} C \left(T_m^{p+1} - T_m^{p} \right) \quad (3.11)$$

The heat flow into the elemental volume of a general interior node m involves heat conduction from the two sides of the volume of the element. The transient finite difference formulation for an interior node can be expressed as;

$$kA \frac{T_{m+1} - T_m}{\Delta x} + kA \frac{T_{m-1} - T_m}{\Delta x} = \rho A \Delta x C \frac{T_{mp+1} - T_{mp}}{\Delta t} \quad (3.12)$$

Expressing the interior node equation in an implicit finite difference form is given as;

$$T_m^p = F_{oj} T_m^{p-1} + (1 - 2F_{oj}) T_m^{p+1} + F_{oj} T_m^{p-1} \quad (3.13)$$

Where;

F_o = dimensionless mesh Fourier number

The formulation of the convection boundary condition at the right boundary (node m) for the implicit case is given as;

$$hA\left[t_{sol-air(t)} - T_{mp,1}\right] + kA\left[\frac{T_{mp+1,1}-T_{mp,1}}{\Delta x}\right] = \rho A\frac{\Delta x}{2} C\frac{T_{mp,1}-T_{mp}}{\Delta t} \quad (3.14)$$

The general finite difference equation derived for the right boundary (node m) on the outdoor surface is given as;

$$T_{mp,1} = 2F_{om}\left[\frac{h_i k}{\Delta x}\right]_M + 2F_{om}\left[t_{sol-air(t)}\right] + \left[1 - 2F_{om}\left(\frac{h_i k}{\Delta x}\right)_1 - 2F_{om}\right]T_{mp,1} + 2F_{om}T_{mp-1,1} \quad (3.15)$$

Similar analogy is used to derive the formulation of the convection boundary condition at the left boundary (node 1) for the implicit case and is given as;

$$hA\left[t_i - T_{0p,1}\right] = kA\left[\frac{T_{2p,1}-T_{1p,1}}{\Delta x}\right] + \rho A\frac{\Delta x}{2} C\frac{T_{1p,1}-T_{1p}}{\Delta t} \quad (3.16)$$

$T_{p,1}$

The general finite difference equation for the left boundary (node 1) on the indoor surface and is given as;

$$T_{1p} = 2F_{oi}\left[\frac{h_o k}{\Delta x}\right]_1 + \left[t_i\right] + \left[1 - 2F_{oi} - 2F_{oi}\left(\frac{h_o k}{\Delta x}\right)_1\right]T_{1p,1} + 2F_{oi}T_{2p,1} \quad (3.17)$$

The general finite difference derived for the interface nodes between layers is given as;

$$BT_i = \left[\frac{k_j}{\Delta x_j}\right]_p T_{ip-1,1} + \left[B - \left(\frac{k_j}{\Delta x_j}\right)_p - \left(\frac{k_{j+1}}{\Delta x_{j+1}}\right)_p\right]T_{ip,1} + \left[\frac{k_{j+1}}{\Delta x_{j+1}}\right]_p T_{ip+1,1} \quad (3.18)$$

Δx_j

Where B □□□ ________________ρ C Δx$_{j\ j}$ $_j$ □2ρΔ t$_{j\ 1□}$ C$_{j\ 1□}$ Δx $_{j\ 1□}$ □□□

□

The general finite difference equations derived for the left boundary node (node 1), interior nodes inside the layers, interface nodes between the layers and right boundary node on the inside surface (node m) is represented by the general form:

$$a_iT_i = b_iT_{i+1} + c_iT_{i-1} + d_i \qquad 3.19$$

for i=1, 2,…, n. The temperature T_i at a typical node i is linked to the neighbouring temperatures, T_{i+1} and T_{i-1} and previous time step temperature. The coefficients for a_i, b_i, c_i and d_i is given in Table 3.1.

Table 3.1 : Coefficients for the finite difference equation and boundary conditions

TYPE OF NODE	a_i	b_i	c_i	d_i
Left Boundary node (node 1)	$1 + 2F_{01} + 2F_{01}\frac{h_0\Delta x_1}{k_1}$	0	$-2F_{01}$	$T_1^P + (2F_{O_1}\frac{h_0\Delta x_1}{k_1})\, t_i$
Interior node (i) in layer (j)	$1 + 2F_{O_j}$	F_{Oj}	F_{Oj}	T_{mP}
Interface node (i) between layers (j) and (j+1)	$\frac{k_j}{\Delta x_j} + \frac{k_{j+1}}{\Delta x_{j+1}} + B$	$-\frac{k_{j+1}}{\Delta x_{j+1}}$	$-\frac{k_j}{\Delta x_j}$	BT_{mp}
Right Boundary node (node m)	$1 + 2F_{0M} + 2F_{0M}\frac{h_i\Delta x_1}{k_1}$	0	$2F_{0M}$	$T_{mP+1} + (2F_{O_M}\frac{h_i\Delta x_M}{k_M})\, t_{sol-air(t)}$

The indoor temperature and the initial condition were considered to be 25˚C for each of the months. The solar emissivity of the wall was obtained from Al Sanea and Zedan (2001) as 0.4.

The solar absorptivity was obtained from Delgado (2014) as 0.85 for dark coloured surfaces. The thermal performance of the wall configurations was determined for the average day of the month representing the average for the days of the month. The month of March is selected because it has the highest level global radiation and outside dry bulb temperature whiles the month of August is selected because it has the lowest level of global radiation and outside dry bulb temperature for the day.

3.3 Wall composition parameters

The wall composition consisted of different materials arranged in layers. Each layer contained a different material with its associated thermo-physical properties like thermal conductivity, specific heat capacity and density. The thermo-physical properties for the walls were also used as input parameters for the simulation. The thermo-physical properties of the wall materials are shown in Table 3.2. The four wall constructions used are mass concrete block wall, hollow concrete block wall, mud brick wall and sandcrete block wall.

Table 3.2 : Thermo-physical properties of the wall materials

Name	**Thickness** (m)	**Density** $\left(Kg/m^2\right)$	**Specific heat** $\left(J/Kg\,K\right)$	**Thermal Conductivity** $\left(W/m\,K\right)$
Cement plastering	20	1762	840	0.721
Mud brick	150	1731	880	0.750
Mass Concrete Block	150	2300	1000	1.63
Hollow Block	150	1362	840	0.96
Sandcrete Block	150	512	880	0.49

SOURCES**:** (Al-Sanea and Zedan, 2001); (Moss, 2007). (Nayak and Prajapati, 2006)

All the walls were made of three layers. Each of the walls had a first and third layer which consisted of a 20 mm cement-sand plastering and rendering. The second layer comprised of the mass concrete block for the mass concrete block wall, hollow concrete block for the hollow concrete block wall, mud brick for the mud brick wall and the sandcrete block for the sandcrete block wall. The simulation was run using the Mathcad software.

3.4 Computation of time lag and decrement factor

The time lag and decrement factor are computed as follows. The equation used to determine time lag is obtained from Asan (1998) as;

$$t_{Tin\,max} - t_{Tout\,max} \quad (3.20)$$

Where; $t_{Tin\,max}$ = inside surface maximum temperature of the wall (˚C)

$t_{Tout\,max}$ = outside surface maximum temperatures of the wall (˚C)

The equation used to determine the decrement factor of the wall is given as;

$$D.F = \frac{T^{in\,(max)} - T^{in\,(min)}}{T_{out\,(max)} - T_{out\,(min)}} \quad (3.21)$$

Where;

$T_{in\,(max)}$ = maximum inside surface temperature (˚C)

$T_{in\,(min)}$ = minimum inside surface temperature (˚C)

$T_{out\,(max)}$ = maximum outside surface temperature (˚C)

$T_{out\,(min)}$ = minimum outside surface temperature (˚C)

The peak instantaneous transmission is obtained as;

$$q_i = h_i (T_{wi} - T_i) \quad (3.22)$$

3.5 Verification of model

The predicted temperatures by the model are compared with an analytical solution developed by Fathipour and Hadidi (2017). The analytical solution solves the transient heat conduction

equation using Green's function under time dependent boundary conditions for the inner and outer surfaces of the wall. The analytical solution is developed for a common wall structure in the city of Tabriz in Iran using a general and approximate sol-air temperature for the climatic conditions on 4th April, 2016.

Statistical analysis is used to test for agreement between the predicted inner and outer temperatures by the model and temperatures developed from the analytical solution. The three statistical methods used are the Root Mean Square Error (RMSE), Mean Percentage Error (MPE) and the Mean Bias Error (MBE). The equations are given as;

$$RMSE = \sqrt{\frac{1}{n}\sum_{i=1}^{n}(G_{pred} - G_{anal})^2} \quad \text{3.22}$$

$$MPE = \frac{1}{n}\sum_{i=1}^{n}\left(\frac{G_{anal} - G_{pred}}{G_{anal}}\right) \times 100\% \quad \text{3.23}$$

$$MBE = \frac{1}{n}\sum_{i=1}^{n}(G_{pred} - G_{anal}) \quad \text{3.24}$$

Where,

G_{pred} = Predicted temperature Value

G_{anal} = Analytical temperature Value

The RMSE represents zero in the ideal case and smaller values obtained from RMSE indicates a better model performance. A value of MBE and MPE closer to zero is desirable and also

indicates a better model performance. In addition percentage error between -10% and +10% is considered acceptable (Khalil and Shaffie, 2013).

CHAPTER FOUR

4.0 RESULTS AND DISCUSSION

4.1 Chapter Outline

This chapter presents the results from the study. The results include temperature variations at the inner and outer surfaces of the wall and also temperature distribution across the thickness of the wall. Results on time lag, decrement factor, peak transmission load and average inner temperature of the wall configurations for the month of August and March are included in this chapter. The chapter concludes with the verification of results between the numerical model used in study and the analytical solution developed.

4.2 Thermal performance for the month of March

The highest level of global solar radiation was recorded in the month of March with a value of 5.188 kWh/m^2. The solar radiation incident on the vertical surface was 2.473 kWh/m^2. The maximum hourly global solar radiation occurred between 13:00 hrs. and 14:00 hrs. The maximum outdoor dry bulb temperature was 33.88 ˚C and occurred at 16:00 hrs. and the average temperature for the day was given as 28.168 ˚C. The maximum sol-air temperature for the month was obtained as 56.644 ˚C at the time 14:00 hrs. The inside and outside heat transfer coefficients were calculated to be 8.228 W/m^2K and 12.249 W/m^2K from Equation 3.3 and 3.4.

4.2.1 Temperature variations at the inner and outer surfaces of mass concrete

block wall for March

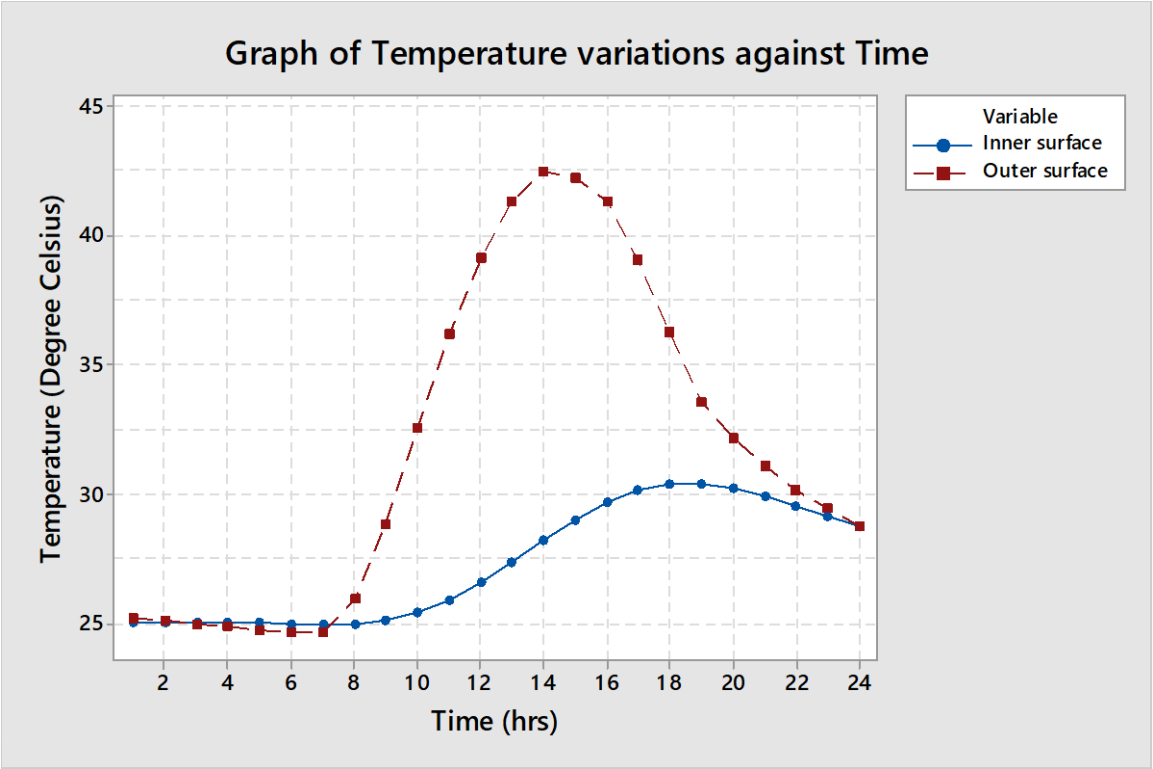

Figure 4.1: Temperature variations at the inner and outer surfaces for mass concrete block wall in March

The temperature variation at the inner and outer surfaces of mass concrete block wall is shown in Figure 4.1. Figure 4.1 shows that the temperature variations at the inner and outer surfaces take a sinusoidal pattern like the variation of the outside dry bulb temperature and global radiation. The temperature at the inner and outer surfaces decreases from 1:00 hrs. to 7:00 hrs. due to decreasing outside dry bulb air temperature. The minimum temperature for both surfaces occurs at 7:00 hrs. The temperature at the outer surface rises from 7:00 hrs. to 14:00 hrs. where a maximum temperature of 42.455 ˚C is obtained whiles the inner surface temperature rises from 7:00 hrs. to 18:00 hrs. where maximum temperature for the inner surface is 30.403 ˚C. The temperatures at the inner and outer surfaces decrease hourly after attaining maximum temperatures. The increasing temperature at the inner surface whiles the temperature at the outer surface is decreasing is due to thermal storage effect of the wall. The time difference

between the maximum inner surface temperature at 18:00 hrs. and maximum outer surface temperature at 14:00 hrs. is four hours. This implies that the time lag for the wall is four hours.

4.2.2 Temperature distribution across the thickness of the mass concrete block wall for March

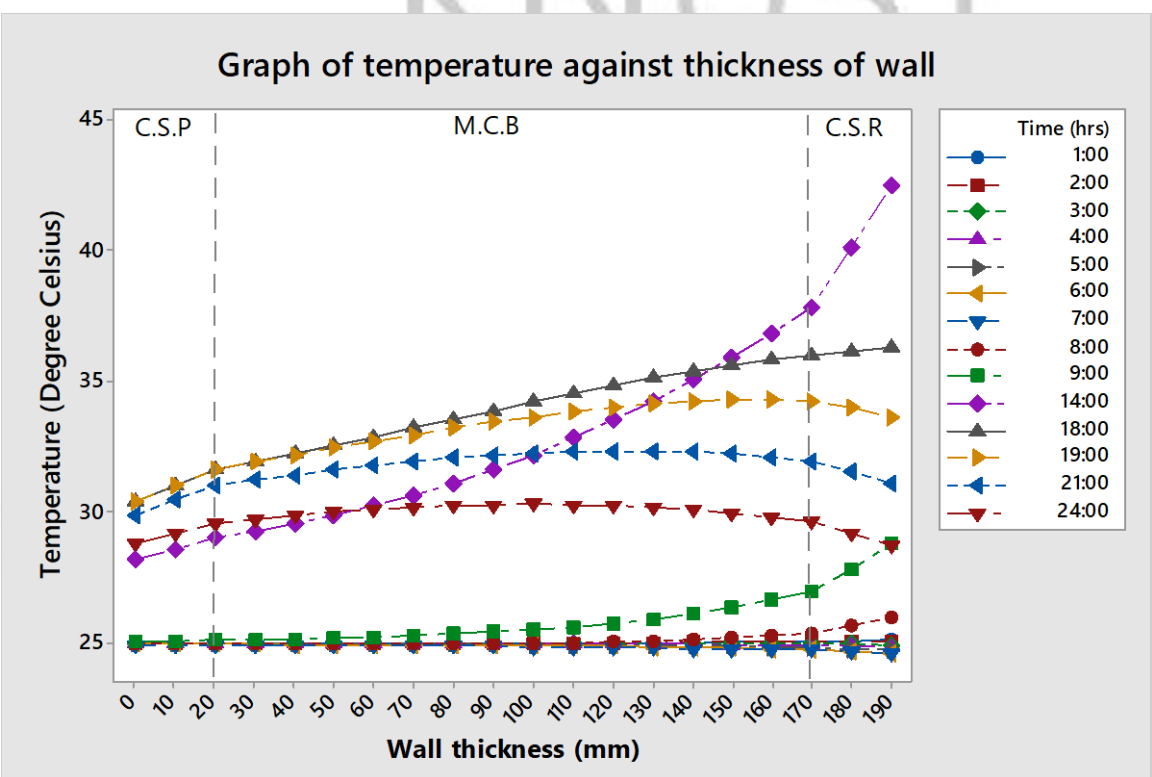

Figure 4.2: Temperature distribution across the wall thickness at various times for mass concrete block wall for March

The temperature distribution across the wall thickness at various times for mass concrete block wall is shown in Figure 4.2. The inner surface of the wall corresponds to the left side of the figure. The temperature variation across the wall thickness has discontinuities at wall thickness 20mm and 170mm respectively which are the interfaces between the layers. The discontinuities at the interfaces are due to different thermal conductivities between the layers. The temperature gradient across the cement-sand rendering (C.S.R) from 1:00 hrs. to 2:00 hrs. is positive due to the initial condition of the wall and then reverses from 3:00 hrs. to 7:00 hrs. due to decreasing outside dry bulb temperature. It then turns into positive value from 8:00 hrs. to 18:00 hrs. due

to global solar radiation and reverses from 19:00 hrs. to 24:00 hrs. when the global solar radiation is absent. The temperature gradient across the mass concrete block (M.C.B) is negative from 3:00 hrs. to 7:00 hrs. and remains positive throughout the day. The cement-sand plastering's (C.S.P) temperature gradient is positive from 1:00 hrs. to 4:00 hrs. which shows heat gain. It then reverses from 5:00 hrs. to 8:00 hrs. due to heat loss at the outer surface and across the mass concrete block. The temperature gradient finally becomes positive from 9:00 hrs. till the end of the day. This shows that the heat stored in the wall gradually dissipates into the room. The average inner surface temperature is 27.329 ˚C which is higher than the designed room temperature by 2.329 ˚C.

4.2.3 Temperature variation of inner and outer surfaces of hollow concrete block wall for March

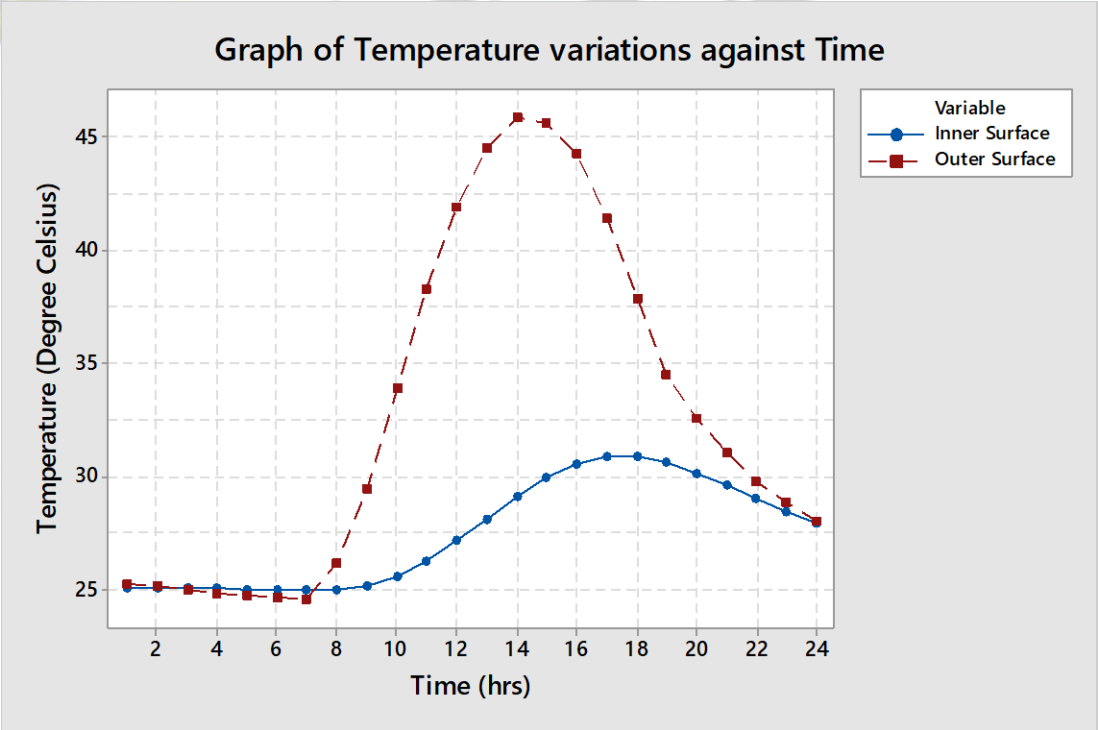

Figure 4.3: Temperature variations at the inner and outer surfaces for hollow concrete block wall for March

The temperature variation at the inner and outer surfaces for hollow concrete block wall is shown in Figure 4.3. The temperature variations show a sinusoidal pattern. The temperatures

at the inner and outer surfaces decrease hourly from 1:00 hrs. to 7:00 hrs. where they both attain minimum values of 24.94 ˚C and 24.55 ˚C respectively. From that time, the temperature at the outer surface increases till 14:00 hrs. where maximum temperature of
45.846 ˚C is obtained. The temperature at the inner surface of the wall increases steadily from 7:00 to 18:00 and attains a maximum value of 30.861˚C. The maximum temperatures at the inner surface at the time 18:00 hrs. is 0.465 ˚C higher than the maximum inner surface temperature of mass concrete block at the same time. The higher temperature at the inner surface may be attributed to the difference in thermal diffusivity of the mass concrete block and hollow block. The time lag for the hollow concrete block is also four hours similar to the mass concrete block and may be attributed to the high level of global radiation and outside dry bulb temperature given in the month of March.

4.2.4 Temperature distribution across the thickness of the hollow concrete block wall for March

The temperature variation across the wall thickness is shown in Figure 4.4. The temperature gradient across the thickness of the cement-sand plastering/rendering follows pattern similar to the mass concrete wall plastering/rendering. The cement-sand rendering (C.S.R) has positive temperature gradient at 1:00 hrs. and 2:00 hrs. It changes to negative from 3:00 hrs. to 7:00 hrs. due to falling outside dry bulb air temperatures. It then has a positive value from 8:00 hrs. to 17:00 hrs. due to global solar radiation and finally turns negative between 18:00 hrs. and 24:00 hrs.

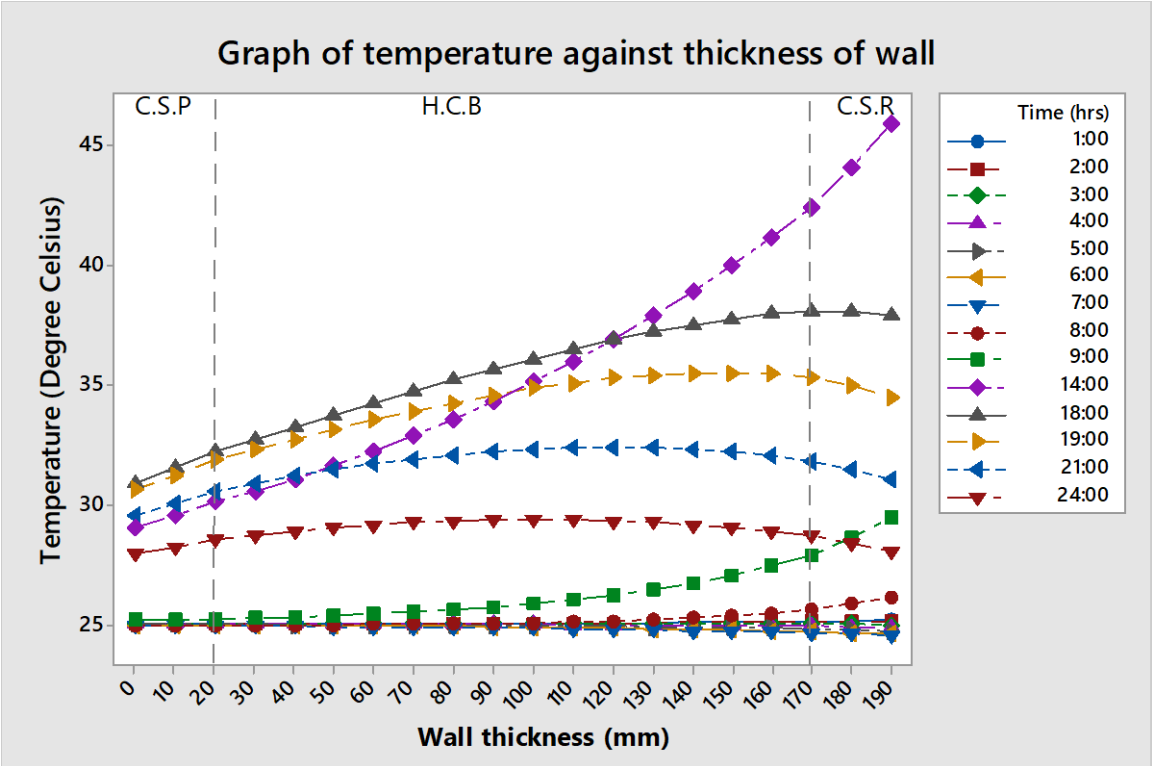

Figure 4.4: Temperature variations across the wall thickness at various times for hollow concrete block wall in March

Furthermore, the temperature gradient across the hollow concrete block (H.C.B) is negative from 3:00 hrs. to 7:00 hrs. and remains positive throughout the day whiles the temperature gradient across the cement-sand plastering (C.S.P) of the wall is positive from 1:00 hrs. to 4:00 hrs. and then changes to negative from 5:00 hrs. to 8:00 hrs. also due to falling outside dry bulb temperature. The temperature gradient finally has positive values from 9:00 hrs. till the end of the day through heat conduction from the hollow concrete block due to heat gain by global solar radiation. The average temperature at the inner surface of the wall is 27.429 ˚C which is higher than the designed room temperature by 2.429 ˚C.

4.2.5 Temperature variations of inner and outer surfaces of mud brick wall The graph of temperature variations of the outer and inner surfaces of mud brick wall is shown in Figure 4.5.

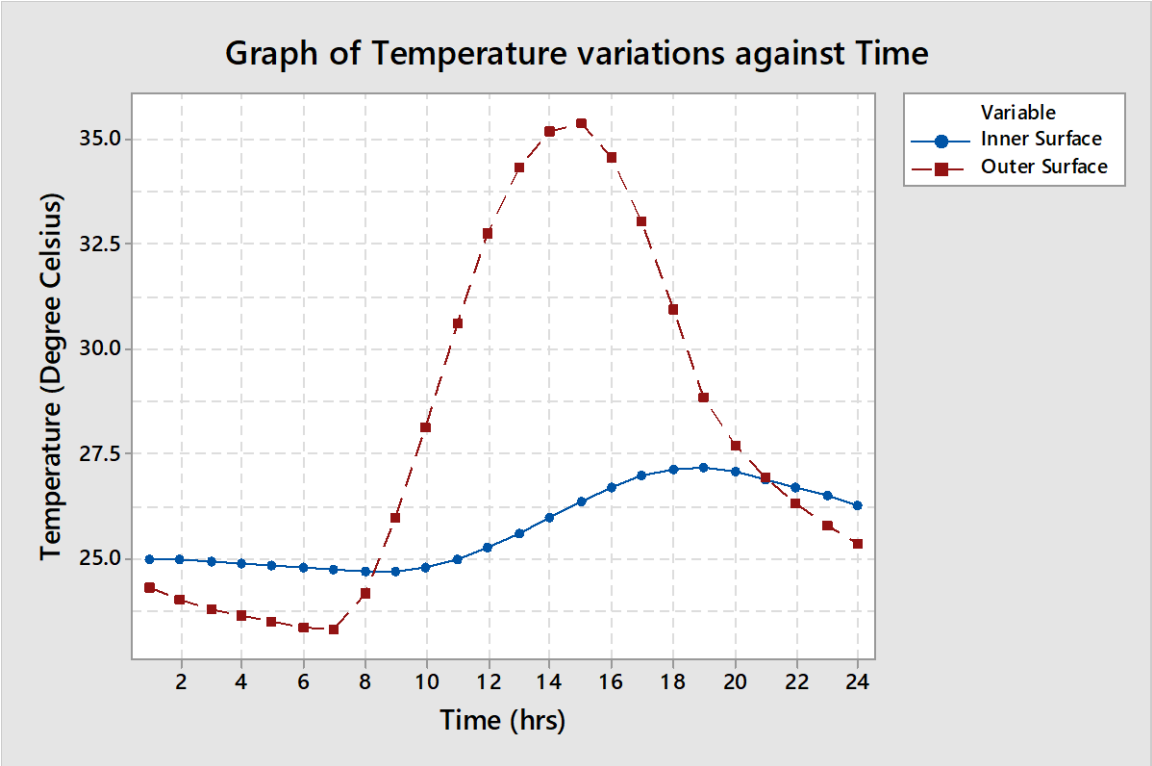

Figure 4.5: Temperature variations at the inner and outer surfaces of mud brick wall for March

The graph shown in Figure 4.5 follows a sinusoidal pattern similar to mass concrete block and hollow concrete block wall. The variation of temperature at the inner surface and outer surface at time 1:00 hrs. to 7:00 hrs. follows similar trends like mass concrete block wall and hollow concrete block wall. The outer surface temperature also rises from 7:00 hrs. to 14:00 hrs. to a maximum value at the same time similar to mass concrete block and hollow concrete block wall. The maximum outer surface temperature is obtained as 45.694˚C and is lower than the maximum outer surface of the hollow concrete block by 0.152 ˚C. The temperature at the inner surface of the wall rises from 7:00 hrs. to 19:00 hrs. instead of 18:00 hrs. like the mass concrete block and hollow concrete block where it attains a maximum value of 29.584 ˚C which is also lower than the maximum inner surface temperature of the mass concrete block wall by 0.819 ˚C and the maximum inner surface temperature of the hollow concrete block wall by 1.284 ˚C. The time lag for mud brick wall is five hours.

4.2.6 Temperature distribution across the thickness of the mud brick wall for March

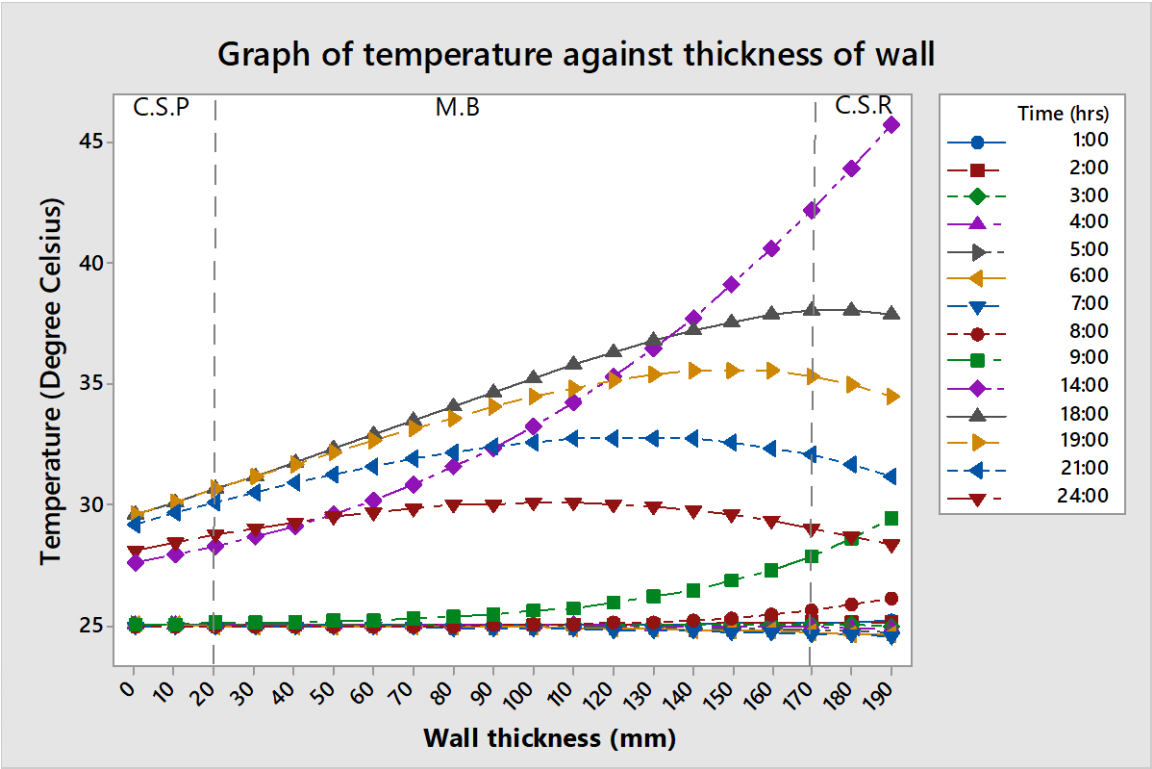

Figure 4.6: Temperature variations across the wall thickness at various times for mud brick wall for March

The temperature distribution across the thickness of mud brick wall shown in Figure 4.6 has less discontinuity in gradient at interfaces because the thermal conductivities of the cementsand plastering/rendering and mud block have similar values at the interfaces unlike the mass concrete block wall. The temperature gradient of the cement-sand rendering (C.S.R) is positive at 1:00 hrs. and 2:00 hrs. It turns negative from 3:00 hrs. to 8:00 hrs. due to decreasing outside dry bulb air temperature and reverses from 9:00 hrs. to 17:00 hrs. due to heat gain from global solar radiation. It then finally turns negative from 18:00 hrs. till the end of the day. The cement-sand plastering (C.S.P) has a positive temperature gradient from 1:00 hrs. to 4:00 hrs. and reverses in sign from 5:00 hrs. to 8:00 hrs. It then has a positive gradient from 9:00 hrs. till the end of the day due to heat conduction from the mud brick. The temperature gradient across the

mud brick (M.B) is negative from 3:00 hrs. to 7:00 hrs. and remains positive throughout the day. The average inner surface temperature is 26.923 ˚C and is higher than the designed room temperature by 1.923 ˚C.

4.2.7 Temperature variation at inner and outer surface of sandcrete wall for March

The graph of temperature variations of the outer and inner surfaces of sandcrete wall is shown in Figure 4.7.

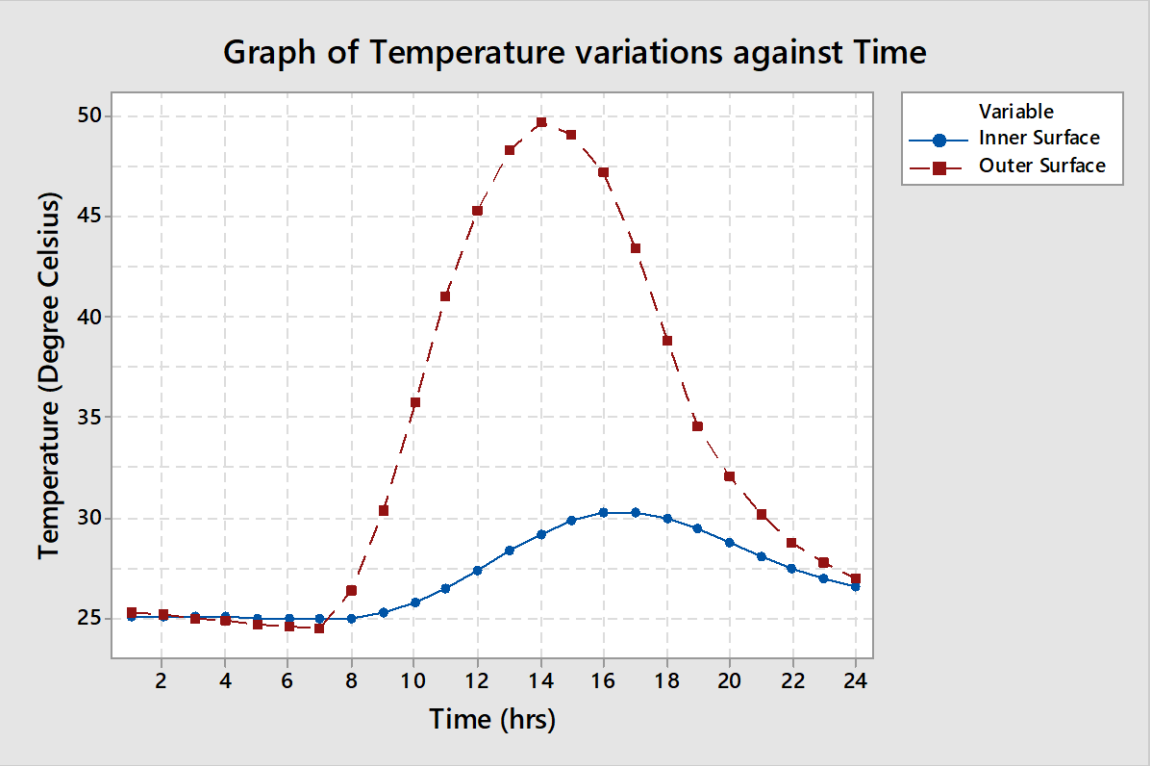

Figure 4.7: Temperature variations at the inner and outer surfaces of sandcrete wall in March

The variation of temperature at the inner surface and outer surface from time 1:00 hrs. to 7:00 hrs. also follows similar trends like mass concrete block wall, hollow concrete block wall and mud block wall. However, the minimum temperature values for inner and outer surface at 7:00 hrs is slightly lower than the minimum temperature of the mass concrete block by 0.027 ˚C and 0.172 ˚C, hollow concrete block wall by 0.01 ˚C and 0.095 ˚C and finally mud block wall by 0.038 ˚C and 0.098 ˚C respectively. The temperature at the outer surface increases

steadily from 7:00 hrs. till 14:00 hrs. to a maximum value which is slightly greater than the maximum temperature at the outer surface of the mass concrete wall by 6.745 ˚C, hollow concrete wall by 3.354 ˚C and mud wall by 3.506 ˚C . The temperature at the inner surface rises from 7:00 hrs. and peaks at 17:00 hrs. instead of 18:00 hrs. like the mass concrete wall and hollow concrete wall or 19:00 hrs. like the mud wall. This may be attributed to the low heat capacity of the sandcrete block. The time lag for the sandcrete wall is three hours.

4.2.8 Temperature distribution across the thickness of the sandcrete block wall for March

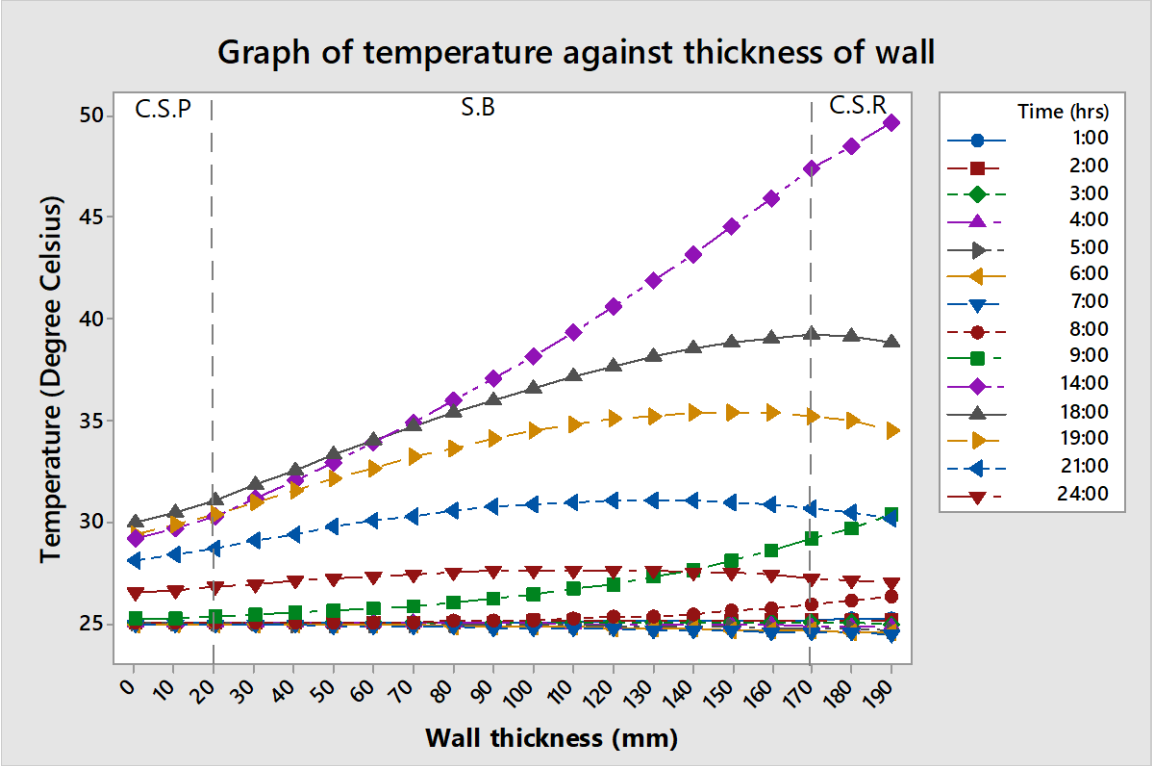

Figure 4.8: Temperature variations across the wall thickness at various times for sandcrete wall for March

The temperature distribution across the thickness of sandcrete wall is shown in Figure 4.8. The temperature gradient at the cement-sand plastering and rendering of the wall follows similar trend like the plastering/rendering of hollow block wall and mud brick wall in the month of March. The temperature gradient of the cement-sand rendering (C.S.R) is positive and negative

during the day and night whiles the cement-sand plastering (C.S.P) has negative temperature gradient only from 5:00 hrs. to 8:00 hrs. after that it has positive temperature gradient throughout the day. The temperature gradient across the sandcrete block (S.B) follows similar trends like the mass concrete block, hollow concrete block and mud brick by having negative gradient from 3:00 hrs. to 7:00 hrs. only. The negative and positive temperature gradient indicates the heat loss and heat gain respectively. The average temperature at the inner surface of the wall is 27.051 ˚C and is higher than the designed room temperature by 2.051 ˚C.

4.3 Thermal performance for the month of August

The lowest level of global solar radiation was recorded in the month of August with a value of 3.065 kWh/m^2. The solar radiation incident on the vertical surface was 1.475 kWh/m^2. The maximum hourly global solar radiation occurred between 13:00 hrs. and 14:00 hrs. The maximum outdoor dry bulb temperature was 27.527 ˚C and occurred at 16:00 hrs. and the average temperature for the day was given as 24.631˚C. The maximum sol-air temperature for the month was obtained as 41.14 ˚C also at the time 14:00 hrs. The inside and outside heat transfer coefficients were calculated to be 8.228 W/m^2K and 12.249 W/m^2K from Equation 3.3 and 3.4.

4.3.1 Temperature variations at the inner and outer surfaces of Mass concrete block wall for August

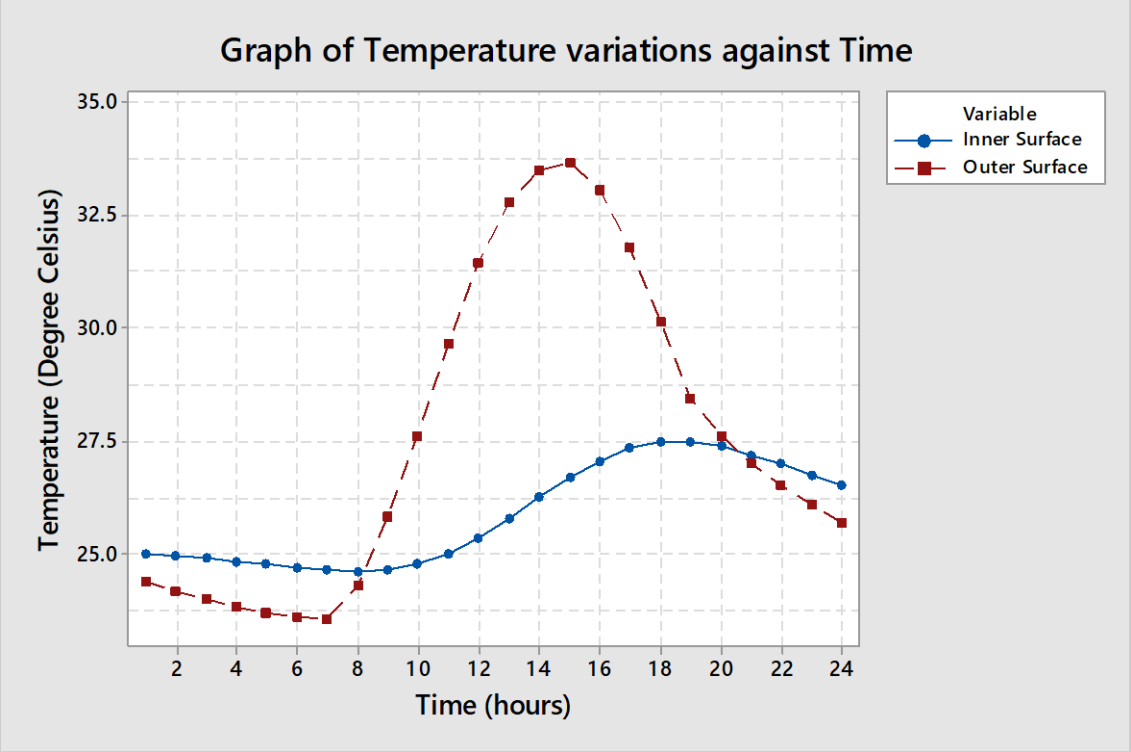

Figure 4.9: Temperature variations at the inner and outer surfaces for mass concrete block for August.

The temperature variation at the inner and outer surfaces for mass concrete block in the month of August is shown in Figure 4.9. The figure shows that the temperature variation at the inner and outer surfaces also follows a sinusoidal pattern. For the month of August, the minimum temperatures at the inner and outer surfaces for the day do not occur at the same time. The temperature at the outer surface drops from 1:00 hrs. to 7:00 hrs. to a minimum value of 23.56 ˚C whiles the temperature at the inner surface drops from 1:00 hrs. to 8:00 hrs. to a minimum value of 24.617 ˚C. The temperatures at the outer surface of the wall then increase hourly from the time 7:00 hrs. till 15:00 hrs. and attain a maximum temperature of 33.687 ˚C which is an hour after sol-air temperature attains maximum value. The temperature at the inner surface rises from 8:00 hrs. to a maximum value of 27.491˚C at 19:00 hrs. The maximum temperature at the inner and outer surfaces of the mass concrete block wall in the month of August is lower than

the maximum inner and outer surface of the wall in the month of March. The lower temperature at the inner and outer surfaces in the month of August compared to March may be attributed to the low level of global solar radiation and outside dry bulb temperature. The time lag for the wall in August is four hours which is the same as the time lag of the mass concrete block in the month March.

4.3.2 Temperature distribution across the thickness of the mass concrete block wall for August

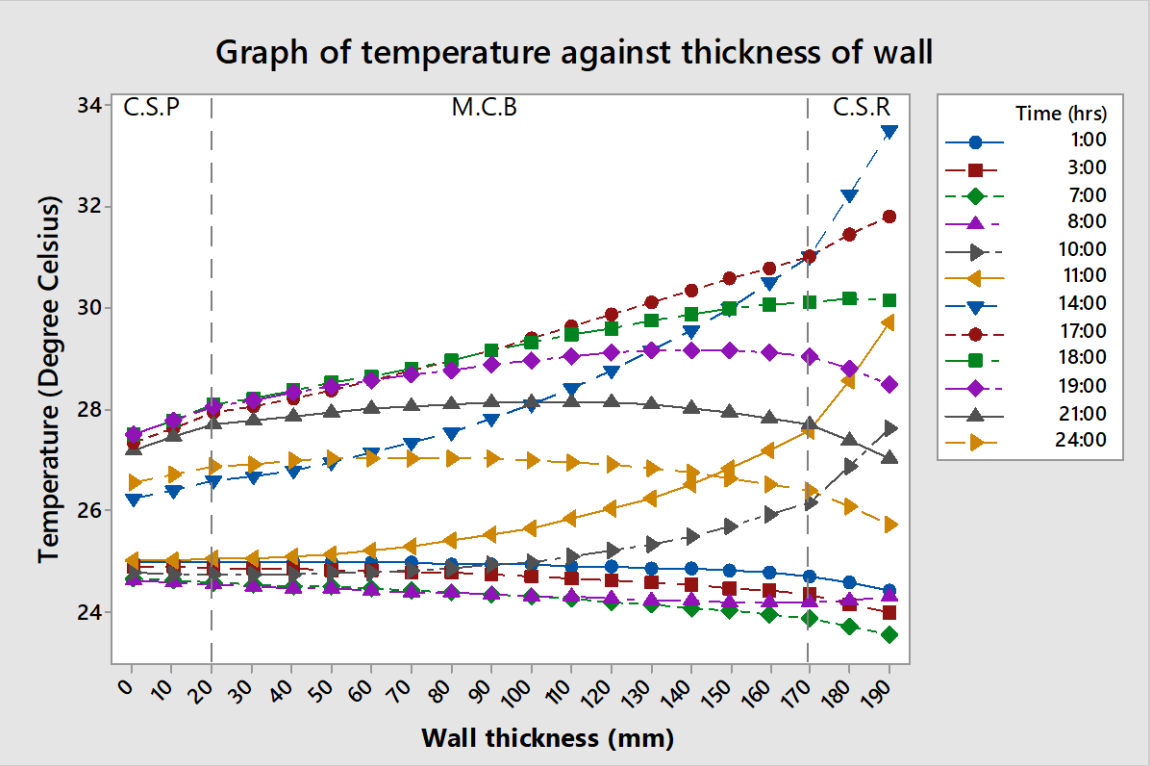

Figure 4.10: Temperature variations across the wall thickness at various times for mass concrete block for August

The temperature discontinuities at the interfaces between the layers due to the different thermal conductivities also occur in the month of August. The temperature gradient at the cement-sand rendering (C.S.R) is negative from 1:00 hrs. to 7:00 hrs. It becomes a positive from 8:00 hrs. to 17:00 hrs. due to heat gain from global solar radiation. The temperature gradient changes to negative from 18:00 hrs. till the end of the day due heat loss from the outer surface of the wall. The temperature gradient across the mass concrete block (M.C.B) is negative from 1:00 hrs. to

8:00 hrs. and reverses to from 9:00 hrs. to 20:00 hrs. The cementsand plastering (C.S.P) has a negative temperature gradient from 1:00 hrs. to 10:00 hrs. even though the cement-sand rendering has a positive temperature gradient from 9:00 hrs. to 10:00 hrs. This shows that it takes time before heat is conducted to the cement-sand plastering (C.S.P). The temperature gradient of the cement-sand plastering (C.S.P) changes to positive from 11:00 hrs. till the end of the day. This indicates that stored heat from the mass concrete block is gradually released to the cement-sand plastering (C.S.P). The average temperature at the inner surface is 25.884˚C and is higher than the designed room temperature by 0.884 ˚C.

4.3.3 Temperature variations at the inner and outer surfaces of hollow concrete block wall for August

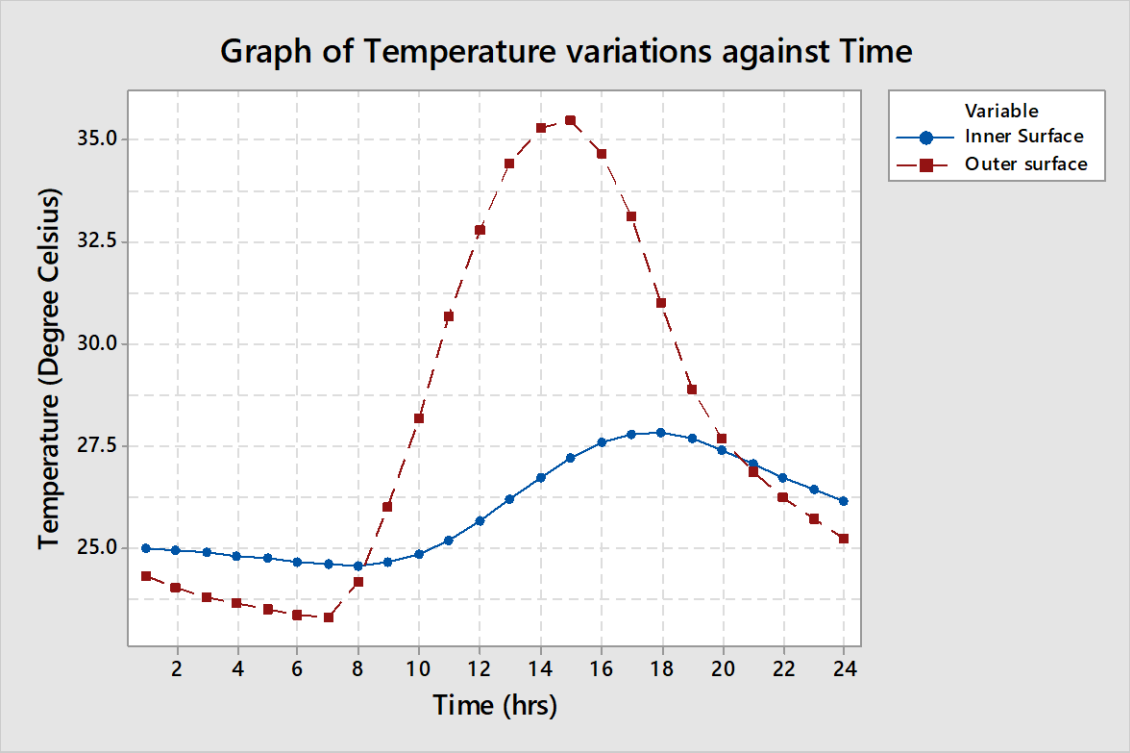

Figure 4.11: Temperature variations at the inner and outer surfaces for hollow concrete block wall for August.

The temperature variation at the inner and outer surfaces for hollow concrete block wall is shown in Figure 4.11. The temperature at the outer surface decreases from 1:00 hrs. till 6:00 hrs. in the morning whiles the temperature at the inner surface decreases from 1:00 hrs. till 8:00

hrs. similar to the mass concrete block in the month of August. From that time, the temperature at the outer surfaces increases to 15:00 hrs. where maximum temperature of 35.456˚C is attained. The temperature at the inner surface of the wall also increases from 8:00 hrs. to 18:00 hrs. to a temperature value of 27.811 ˚C. The temperature variation of the inner and outer surfaces of the hollow concrete block wall in the month of August is also comparatively lower than the month of March.

The time lag for the hollow concrete block in the month of August is three hours which is also lower than the time lag of the wall in the month of March. This suggests that the variation of global solar radiation and outside dry bulb temperature influences the time lag of the wall.

4.3.4 Temperature distribution across the thickness of the hollow concrete block wall for August

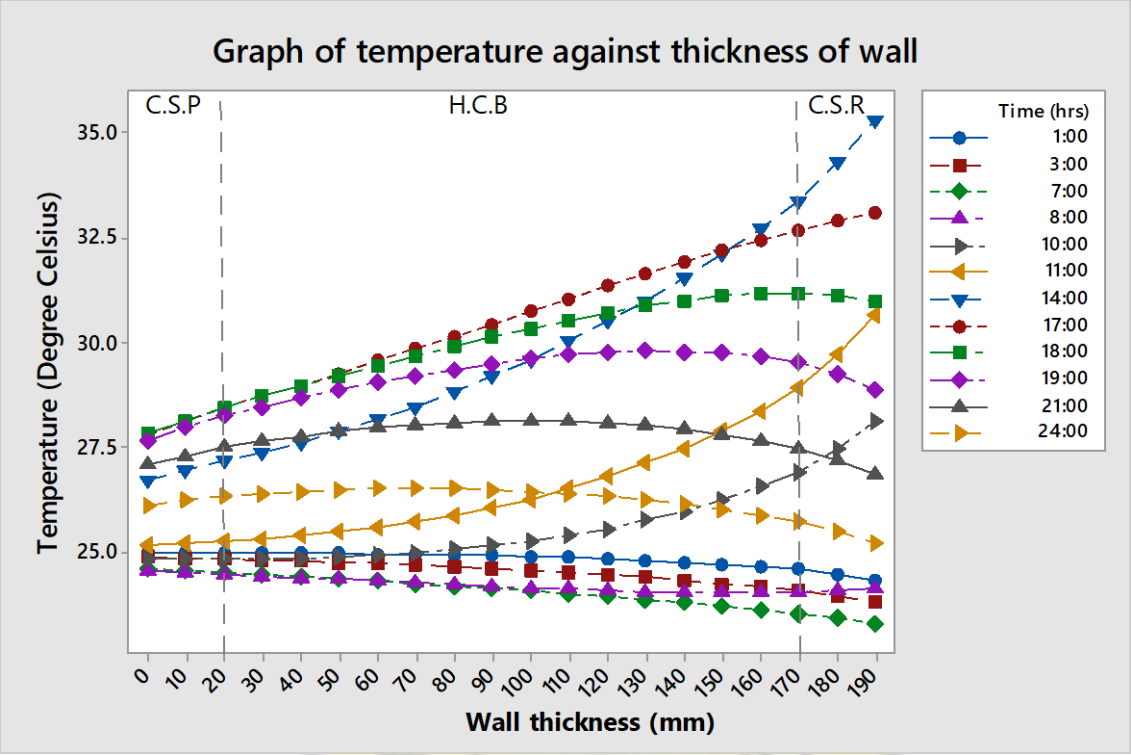

Figure 4.12: Temperature variations across the wall thickness at various times for hollow concrete block wall for August.

The temperature variation across the wall thickness is shown in Figure 4.12. The temperature gradient across the cement-sand plastering and rendering of the hollow concrete wall follows pattern similar to the plastering and rendering of mass concrete wall for the month of August. The cement-sand rendering (C.S.R) has a negative temperature gradient from 1:00 hrs. to 7:00 hrs. due to falling outside dry bulb temperature. Heat gain by the outer surface of the wall changes the temperature gradient at the cement-sand rendering into a positive from 8:00 hrs. to 17:00 hrs. The temperature gradient reverses to a negative sign from 18:00 hrs. till the end of the day due to heat loss from the outer surface. The temperature gradient across the hollow concrete block (H.C.B) is negative from 1:00 hrs. to 8:00 hrs. and also from 21:00 hrs. to 24:00 hrs. The temperature gradient at the cement-sand plastering (C.S.P) is negative from 1:00 hrs. to 10:00 hrs. and becomes a positive from 11:00 hrs. till the end of the day due to stored heat from the hollow concrete block being conducted to the inner plaster. The average inner surface temperature is 25.954 ˚C and is higher than the designed room temperature by 0.954 ˚C and also slightly higher the average inner surface temperature of the concrete block wall by 0.07 ˚C.

4.3.5 Temperature variations at the inner and outer surfaces of Mud brick wall

for August

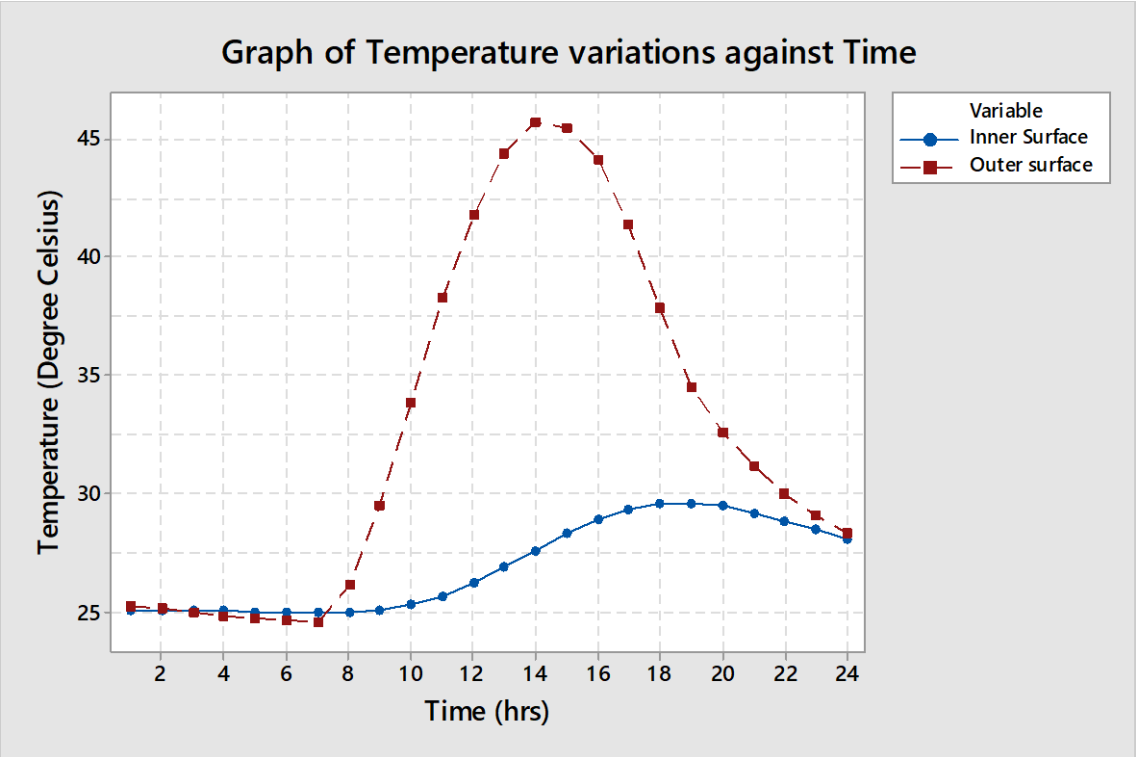

Figure 4.13: Temperature variations at the inner and outer surfaces of mud brick wall for August.

The graph of temperature variations of the outer and inner surfaces of mud brick wall is shown in Figure 4.13. The variation of temperature from the time 1:00 hrs. to the time the inner and outer surfaces of the wall attain minimum temperatures follow pattern similar to mass concrete block and hollow concrete blocks in the month of August. The outer surface temperature also rises from 7:00 till 15:00 hrs. to a maximum value of 35.359 ˚C. The temperature at the inner surface rises by from 8:00 hrs. to 19:00 hrs. where it peaks at value of 27.14 ˚C. The maximum temperature at the inner surface is slightly lower than the maximum inner surface temperature of the mass concrete wall by 0.357 ˚C and the hollow block wall by 0.671 ˚C. The time lag for mud brick wall is four hours and is a reduction in value by an hour when compared to the time lag of the mud brick wall in the month of

March.

4.3.6 Temperature distribution across the thickness of mud brick wall for August

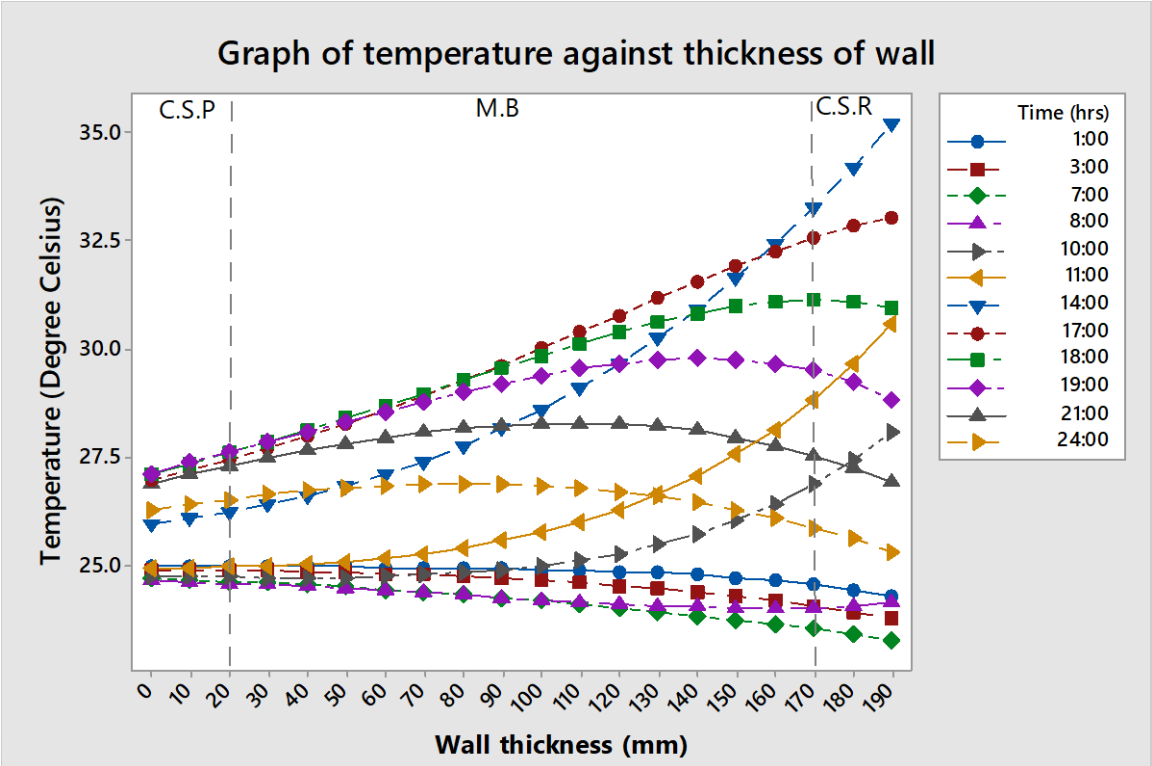

Figure 4.14: Temperature variations across the wall thickness at various times for mud brick wall for August.

The temperature distribution across the thickness of mud brick wall shown in Figure 4.14 has the least discontinuity in the temperature gradient at interfaces compared to the mass concrete block and hollow concrete block wall in the month of March. The temperature gradient across the cement-sand rendering (C.S.R) is negative from 1:00 hrs. to 7:00 hrs. similar to the mass concrete and hollow block wall. The sign of the temperature gradient changes into positive through heat gain from the outer surface due to global solar radiation. The heat loss from the outer surface from 18:00 hrs. to 24:00 hrs. changes the temperature gradient to negative. The temperature gradient across the mud brick (M.B) is negative from 22:00 hrs. to 24:00 hrs. and also from 22:00 hrs. to 24:00 hrs. The cement-sand plastering's (C.S.P) temperature gradient is negative from 1:00 hrs. to 10:00 hrs. The temperature gradient changes to a positive from 11:00 hrs. till the end of the day. This is attributed to heat being conducted to the cement-sand plastering from the mud brick. The average inner surface temperature is 25.737 ˚C and is higher

than the designed room temperature by 0.737 ˚C but lower than the average inner surface temperature of the mass concrete by 1.853 ˚C and hollow block wall by 1.783 ˚C.

4.3.7 Temperature variation at inner and outer surface of sandcrete wall for August

The graph of temperature variations of the outer and inner surfaces of sandcrete wall is shown in Figure 4.15.

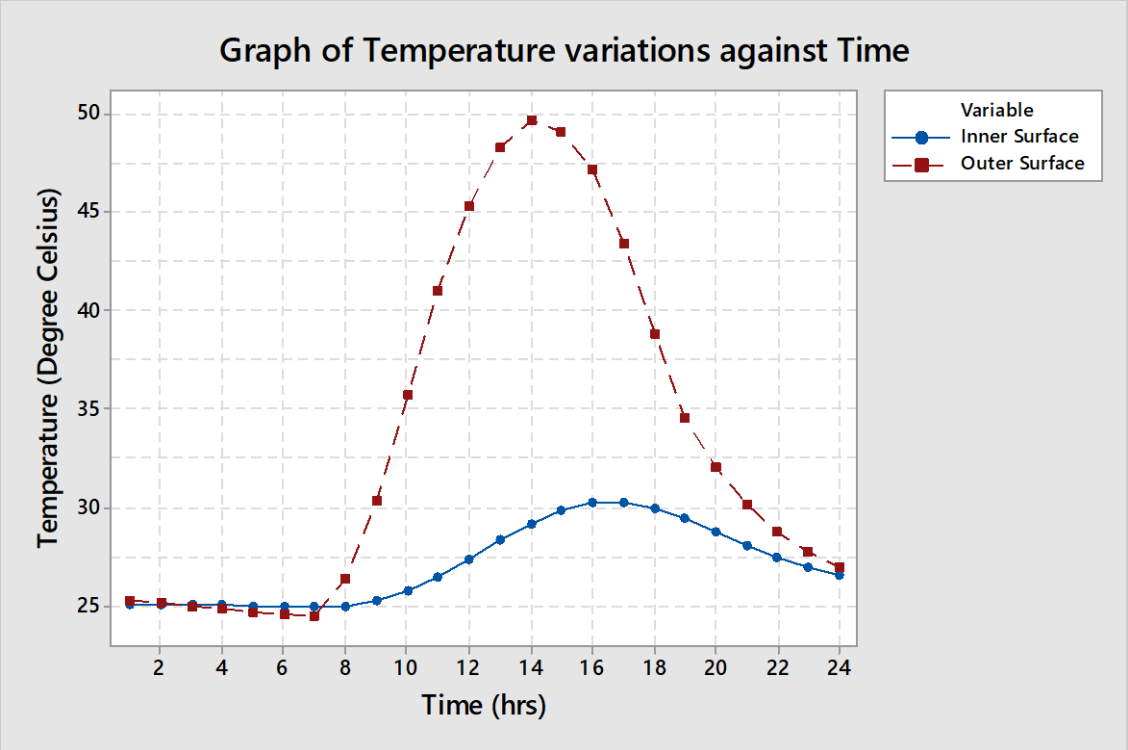

Figure 4.15: Temperature variations at the inner and outer surfaces of sandcrete wall for August

The temperature at the outer surface drops hourly till it reaches a minimum value of 23.025 ˚C at 7:00 hrs. similar to the other walls. However, the minimum temperature value for inner surface occurs at 7:00 hrs. instead of 8:00 hrs. like the other three walls. The outer surface temperature has the lowest minimum value among the three walls. The temperature at the outer surface increases from 7:00 hrs. to 14:00 hrs. to a maximum value of 37.36 ˚C. The temperature at the inner surface also rises from 7:00 hrs. and peaks at 17:00 hrs. instead of 19:00 hrs. like the mass concrete wall and mud block wall or 18:00 hrs. like the hollow concrete wall. The

time it takes the inner surface temperature to peak in the month of August is the same as the month of March. This may be attributed to the heat capacity of the sandcrete block. The time lag for the sandcrete wall is two hours.

4.3.8 Temperature distribution across the thickness of the sandcrete block wall for August

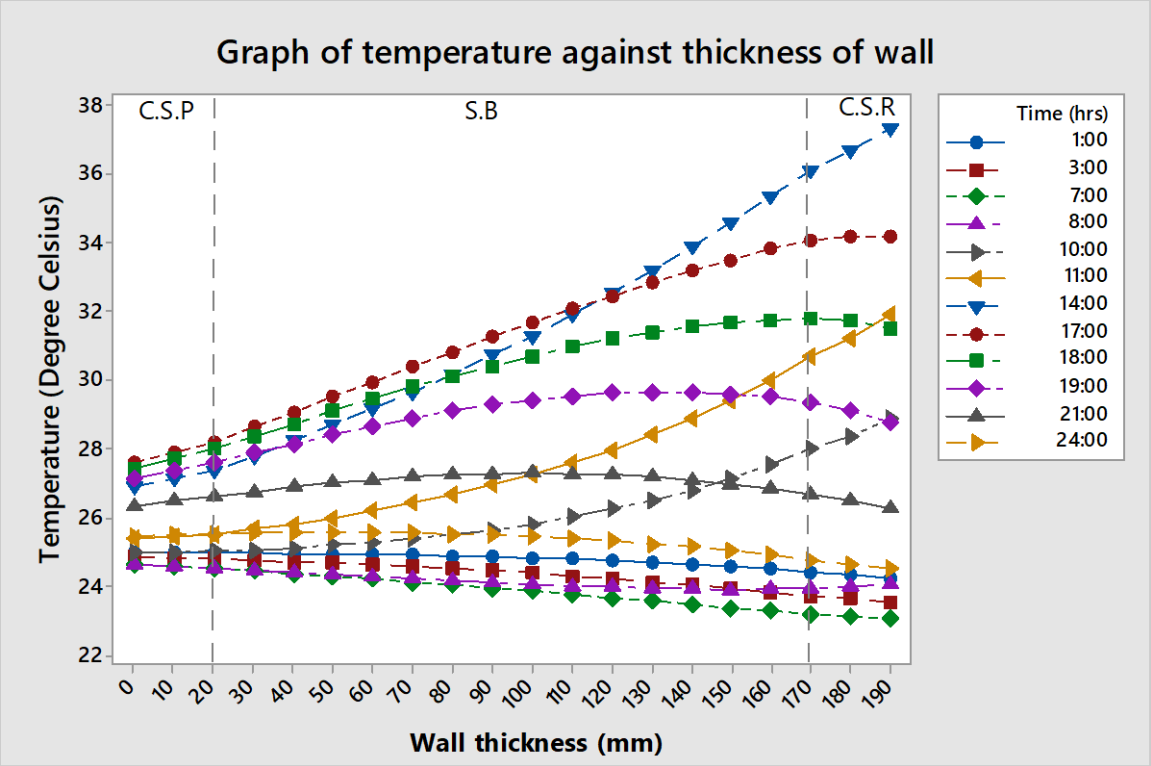

Figure 4.16: Temperature variations across the wall thickness at various times for sandcrete wall for August

The temperature distribution across the thickness of sandcrete wall is shown in Figure 4.16. The temperature gradient at the inner and outer plaster of the wall follows similar trend like the mass concrete, hollow block and mud brick wall in the month of August. The temperature gradient across the cement-sand rendering (C.S.R) is positive and negative during the day and night at the same time similar to the other walls. The cement-sand plastering (C.S.P) has negative temperature gradient only from 1:00 hrs. to 9:00 hrs. instead of 10:00 hrs. like the mass concrete, hollow and mud brick walls but has positive values throughout the day. This indicates that heat conduction from the sandcrete block (S.B) to the cement-sand plastering

(C.S.P) is faster than the other walls after heat gain from the outer surface through global radiation. The average temperature at the inner surface of the wall is 25.807 ˚C and is higher than the designed room temperature by 0.807 ˚C. It is also slightly lower than mass concrete and hollow concrete wall but infinitesimally higher than the mud brick wall.

4.4 Impact of time lag on wall configuration

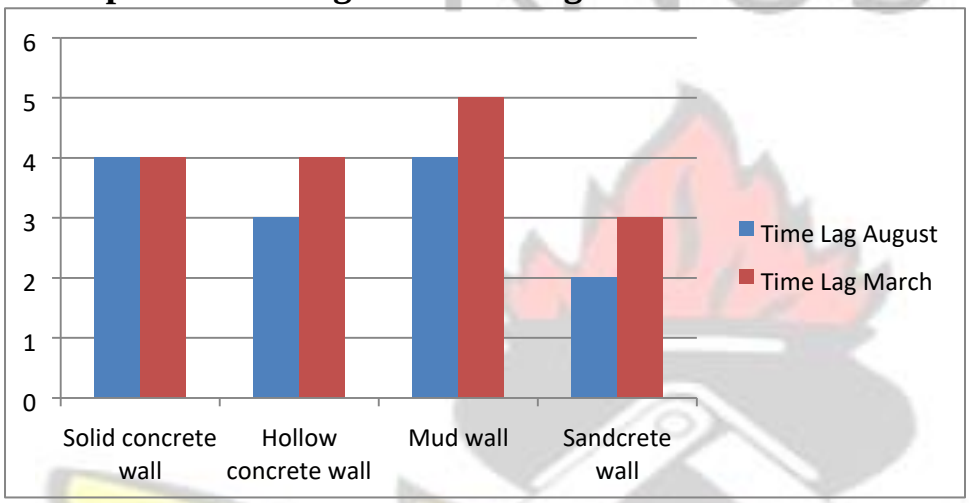

Figure 4.17: Time lag of the walls in the months of August and March

The impact of time lag on the various wall configurations is shown in the Figure 4.17. The highest time lag value is attained by the mud brick wall in the month of March whiles the lowest time lag is obtained by the sandcrete block wall in the month of August. The difference in time lags of the wall is influenced by the heat capacity of wall, variation of global solar radiation and outside dry bulb temperature (Oktar et al, 2016). The time lag value for the walls in the month of August is reduced by an hour for the hollow concrete wall, mud wall and sandcrete wall when compared to their time lag values in the month of March. This may also be attributed to the lower global solar radiation and outside dry bulb temperature for the month of August. However, the time lag of the mass concrete block remains the same in both months. The time lag value of the sandcrete block is lowest among the walls in the month of March and August may be attributed to the low heat capacity of the sandcrete block.

4.5 Impact of decrement factor on wall configuration

The decrement factor of the walls in the months of August and March is shown in Figure 4.18. The decrement factor indicates the ability of the wall to reduce the amplitude of the temperature wave of the outer surface to that of the inner surface. The decrement factor for each of the walls is different for both months. The lowest decrement factor is 0.204 and it occurs in the month of August for the mud brick wall whiles the highest decrement factor occurs in the month of March for the Mass concrete wall and has a value of 0.305. Similarly, the high decrement values for the other walls also occur in the month of March whiles the low decrement values for the month occur in August.

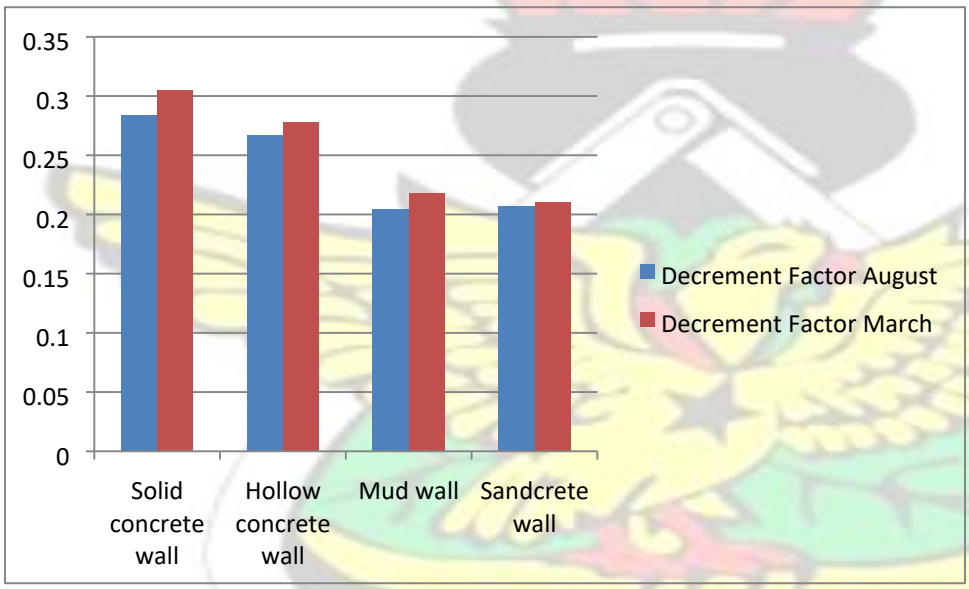

Figure 4.18: Decrement factor of the walls in the months of August and March

The difference in value of the decrement factor for the mass concrete wall in the month of March when compared to August is 0.021. The difference in value of the decrement factor for the hollow concrete wall in March when compared to August is 0.011. Similar reduction values are given by mud and sandcrete wall as 0.014 and 0.003 respectively. This means that the mass concrete block has a slightly better reduction in decrement factor value from the month of March to August compared to the other walls.

4.6 Peak load of the wall configuration

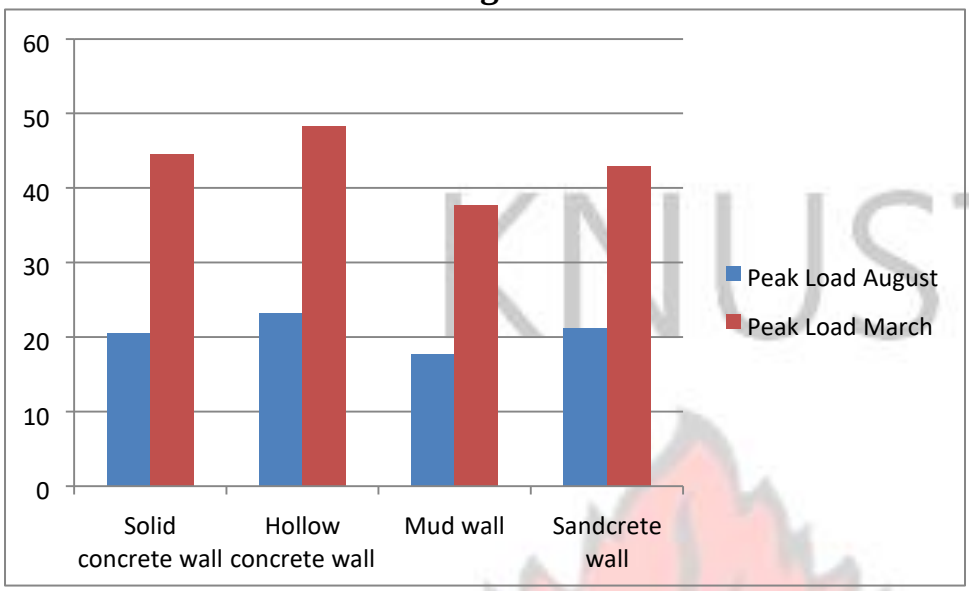

Figure 4.19: Peak transmission loads of the walls in the month of August and March

The peak transmission loads of the various walls are shown in Figure 4.19. The mud brick wall has the lowest peak transmission loads in both months while the highest peak loads is given by the hollow concrete wall. The mass concrete wall has a higher peak load than the sandcrete wall in the month of March but this reverses slightly in the month of August. The peak transmission load in the month of August is almost half of the peak load in March. This means that the variation of the global solar radiation and outside dry bulb temperature of a particular month affects the peak transmission load of the wall.

4.7 Inner surface temperature of the wall configuration

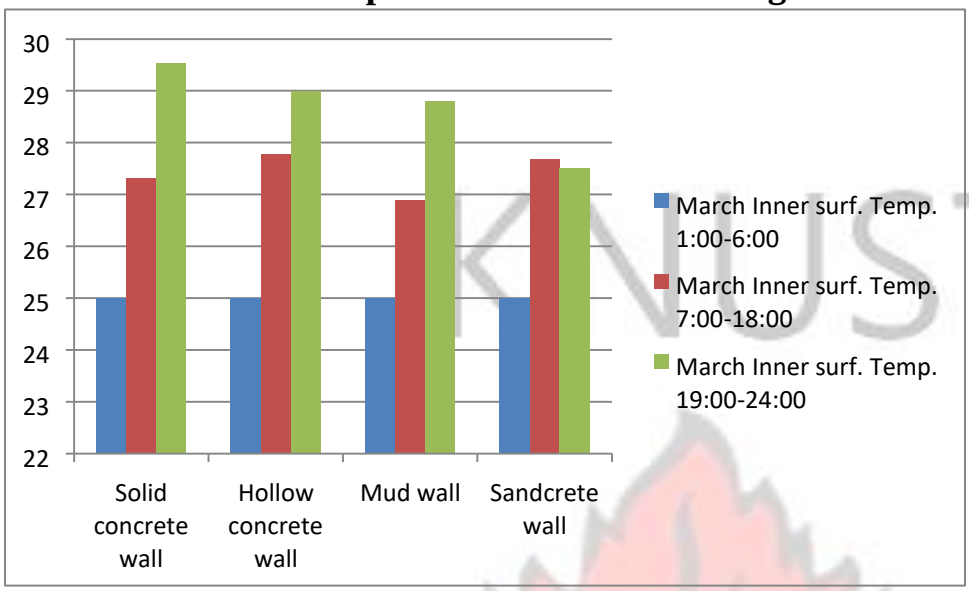

Figure 4.20: Average inner surface temperature for various time intervals in March

The average inner surface temperature for the time periods 1:00-6:00 hrs., 7:00-18:00 hrs. and 19:00-24:00 hrs. is shown in Figure 4.20 for the month of March. The time interval 1:006:00 hrs. and 19:00-24:00 hrs. represents the time period when global solar radiation is absent whiles the time interval 7:00-18:00 hrs. represents the time period when global solar radiation is present. The lowest average temperature between the time periods of 7:00-18:00 hrs. when there is global solar radiation is given by the mud brick wall whiles the highest temperature is given by hollow concrete block wall and is followed closely by the sandcrete block. The highest average inner surface temperature for the 24 hour period is obtained during 19:0024:00 hrs for the mass concrete wall, hollow concrete wall and mud brick wall when global solar radiation is absent. This is attributed to time lags of the walls. The highest average inner surface temperature for this time period is given by mass concrete block whiles the lowest temperature is given by the sandcrete block wall.

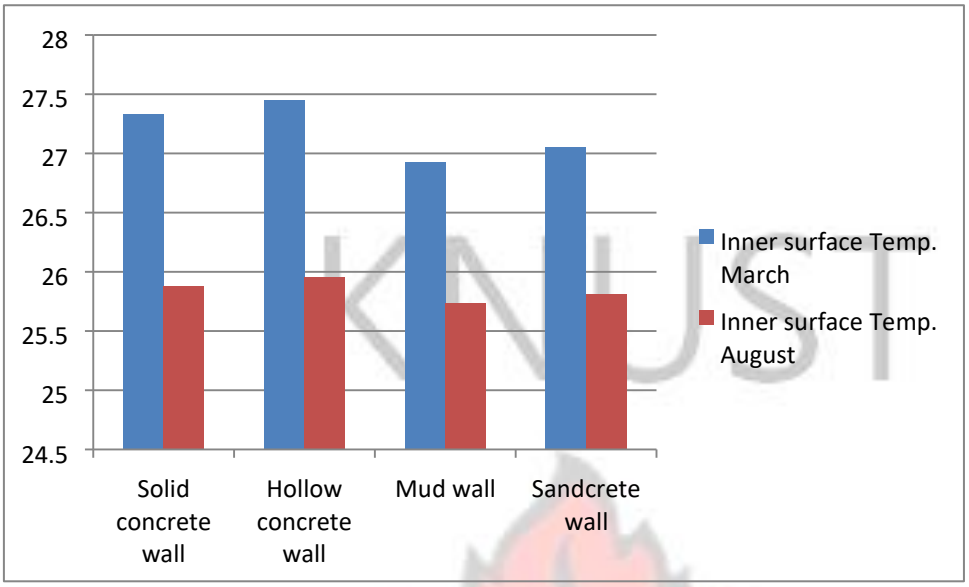

Figure 4.21: Average Inner surface temperature of the walls in the months of August and March

The variation of the inner surface temperature for the day is averaged for each of the months and is shown in Figure 4.21. The figure shows that the mud has lowest average inner surface temperature for August and March as 26.93 ˚C and 25.737 ˚C respectively. The highest average inner temperature is given by the hollow block in the month of August as 24.954 ˚C and March as 27.453 ˚C. In addition, the highest average inner temperature of the walls is found in the month of March and the lowest values in the month of August. This is attributed to heat gain through the high level of global solar radiation and outside dry bulb air temperature recorded for March and also the low level of global radiation and outside dry bulb temperature recorded for August. The low average temperatures obtained in the month of August indicates that the temperature at the inner surface of the wall does not fluctuate too much from the designed temperature of 25 ˚C in the room.

4.8 Verification of results

The predicted temperature values were validated with an analytical solution developed by Fathipour and Hadidi (2017). The values of the temperature variation at the inner and outer surfaces of the wall with time developed by the analytical solution are compared with the predicted inner and outer surface temperatures by the model and are shown in Figure 4.22.

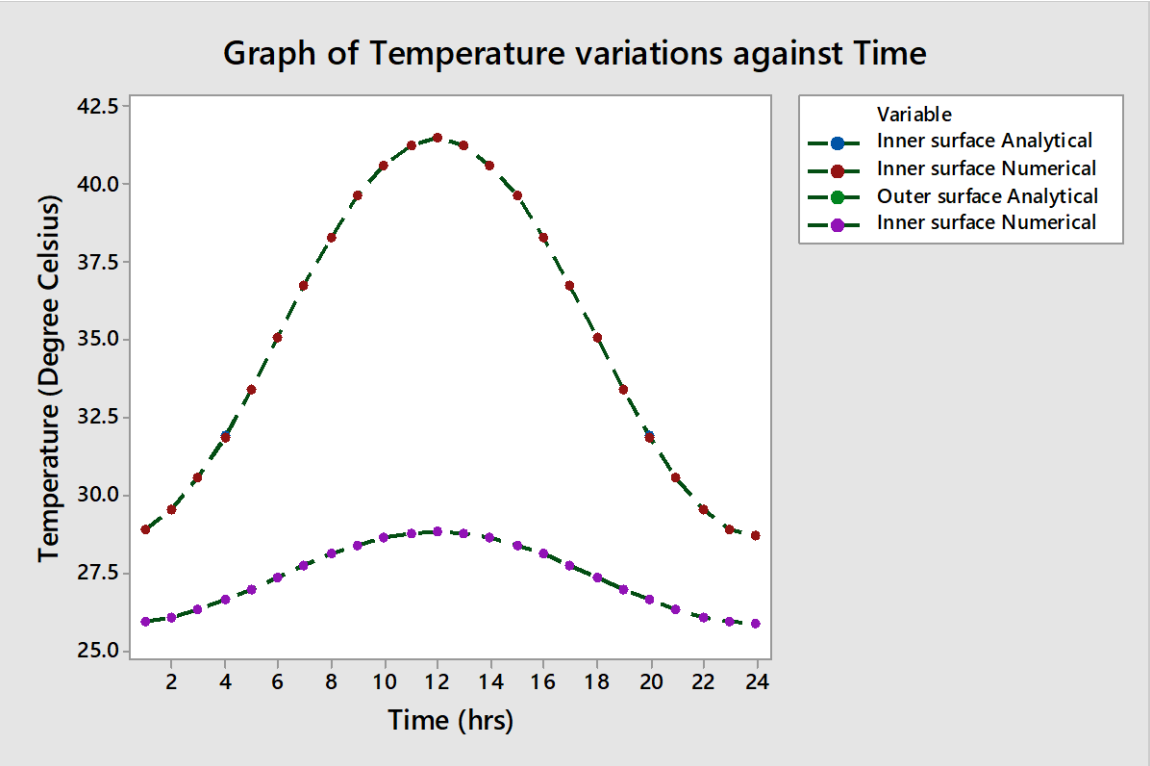

Figure 4.22: Comparison of temperature variations at inner and outer surfaces with time

The Root Mean Square Error (RMSE), Mean Percentage Error (MPE) and the Mean Bias Error (MBE) for the inner surface temperatures are calculated from Equation 3.22 to 3.24 as 0.005, 0.015 and 0.004 respectively. In addition, the same equations are used to calculate for the outer surface temperatures as 0.004, 0.007 and 0.002 respectively. The percentage error falls within the tolerance range. The results show that the predicted temperature values and the analytical solution values are in agreement.

CHAPTER FIVE

5.0 CONCLUSION AND RECOMMENDATION

5.1 Conclusion

A numerical model was used to evaluate the time dependent temperature variation in a mass concrete block wall, hollow concrete wall, mud brick wall and sandcrete block wall using periodic outside dry bulb temperature and global solar radiation. The climatic data was obtained from the K.N.U.S.T solar laboratory for the area of Kumasi.

The results showed that the heat gain by the wall through global solar radiation and outside dry bulb temperature in the climatic area of Kumasi and had an impact on the inner surface temperature, peak transmission load, time lag and the decrement factor of the wall.

The time lag values for the hollow concrete wall, mud wall and sandcrete wall had high values in March when the level of global solar radiation and outside dry bub temperature was high and reduced by an hour in August when the levels were low. The highest time lag was achieved by the mud brick wall which had five hours in the month of March. This was followed by the mass concrete wall which had time lag value of four hours for both months.

The lowest decrement factor value was also given by the mud brick wall as 0.204 in the month of March whiles the lowest decrement factor in the month of August was given by the sandcrete block wall as 0.207 which also followed the mud brick wall closely in March. The decrement factor value varied slightly between wall configurations when comparing the values obtained for March to August.

It may also be concluded that, mud brick reduced temperature fluctuations at the inner surface temperatures slightly better than the other walls by having a low average inner surface temperature for August and March as 25.737 ˚C and 26.923 ˚C respectively.

5.2 Recommendation

The recommendations given for this this study are;

1. Other building wall configurations aside the ones given in this study should be investigated to see the effect of climatic data on the thermal performance of the wall.
2. The climatic conditions of other parts of Ghana should also be used to evaluate the thermal performance of the wall configurations.

REFERENCES

Al-Sanea, S.A. and Zedan, M.F., (2001). Effect of Insulation Location on Initial Transient Thermal Response of Building Walls. J. Therm. Envel. Build. Sci. 24, 275–300. https://doi.org/10.1106/07E7-FGCJ-MFF7-974W. (Accessed: February 21, 2018).

Asan, H. (2006). Numerical computation of time lags and decrement factors for different building materials. Building Environment, 41, 615–620. https://doi.org/10.1016/j.buildenv.2005.02.020. (Accessed: October 20, 2017).

Asan, H. and Sancaktar, Y.S. (1998). Effects of wall's thermophysical properties on time lag and decrement factor. Energy Build. 28, 159–166.

ASHRAE (2009). Handbook of fundamentals. Atlanta, GA: American society of heating, refrigerating and air-conditioning engineers.

Balaji, N.C., Mani, M., and Venkatarama Reddy, B.V. (2013). Thermal performance of the building walls, in: Building Simulation Application 2013, 1st IBPSA Italy Conference. pp. 151–60.

Barber, S. (2012). History of Passive Solar Energy. East Carolina, USA: East Carolina University.

Delgado, J.M.P.Q. (2014). Drying and Wetting of Building Materials and Components. 1st Edition. Switzerland: Springer International Publishing

Duffie, J. A. and Beckman, W. A. (2013). Solar engineering of thermal processes (4th ed.). Hoboken, N.J.: John Wiley and Sons.

Fathipour, R. and Hadidi, A. (2017). Analytical solution for the study of time lag and decrement factor for building walls in climate of Iran. Energy 134, 167–180. https://doi.org/10.1016/j.energy.2017.06.009. (Accessed: October 21, 2017).

Ghana Statistical Service (2014). 2010 Population & Housing Census: District Analytical Report: Kumasi Metropolitan. Ghana statistical service.

GreenSpec: Decrement Delay / Factor in the Building Envelope Fabric [WWW Document], (2017). URL http://www.greenspec.co.uk/building-design/decrement-delay/ (Accessed: March 22, 2017).

Incropera, F.P. and DeWitt, D.P. (1990). Fundamentals of heat and mass transfer. New York: J. Wiley.

Jin, X., Zhang, X., Cao, Y., and Wang, G. (2012). Thermal performance evaluation of the wall using heat flux time lag and decrement factor. Energy Build. 47, 369–374. https://doi.org/10.1016/j.enbuild.2011.12.010. (Accessed: November 18, 2017).

Khalil, S. and Shaffie, A. (2013). Performance of statistical comparison models of solar energy on horizontal and inclined surface. International Journal of Energy and Power, 2(1), pp 8-25.

Kumar, D.S. (2009). Heat and Mass Transfer (Two Colour). New Delhi: S. K. Kataria & Sons.

Lakatos, A. (2017). Measurement of the heat transfer decrement of different wall structures. Fluids, Heat and Mass Transfer, pp 29-34

Li, Y. and Xu, P. (2006). Thermal mass design in buildings–heavy or light? Int. J. Vent. 5, 143–150.

Long, L. and Ye, H. (2015). Effects of Thermophysical Properties of Wall Materials on Energy Performance in an Active Building. Energy Procedia 75, 1850–1855. https://doi.org/10.1016/j.egypro.2015.07.161. (Accessed: May 17, 2018).

Moss, K.J. (2007). Heat and Mass Transfer in Buildings. 2nd ed. New York: Taylor and Francis.

Moujaled, J.K. (2014). A comparative assessment of solar resource databases, simulations and ground observations for Kumasi. Msc thesis, KNUST, Kumasi.

Nayak, J. and Prajapati, J. (2006). Handbook on energy conscious buildings. Pilot Edition. Bombay

Nero, B.F., Callo-Concha, D., Anning, A. and Denich, M. (2017). Urban Green Spaces Enhance Climate Change Mitigation in Cities of the Global South: The Case of Kumasi, Ghana. Procedia Eng. 198, 69–83. https://doi.org/10.1016/j.proeng.2017.07.074. (Accessed: March 22, 2018).

Oktay, H., Argunhan, Z., Yumrutaş, R., Işık, M.Z. and Budak, N. (2016). An investigation of the influence of thermophysical properties of multilayer walls and roofs on the dynamic thermal characteristics. Mugla J. Sci. Technol. 2, 48–54.

Ozel, C. and Ozel, M. (2012a). Effects of Wall Orientation and Thermal Insulation on Time Lag and Decrement Factor. 9th International Conference on Heat Transfer, Fluid Mechanics and Thermodynamics, pp 674-679.

Ozel, M. and Ozel, C. (2012b). Comparison of Thermal Performance of Different Wall Structures, 9th International Conference on Heat Transfer, Fluid Mechanics and Thermodynamics, pp 680-684.

Reilly, A. and Kinnane, O. (2017). The impact of thermal mass on building energy consumption. Journal of Applied Energy, 198, 108–121. https://doi.org/10.1016/j.apenergy.2017.04.024. (Accessed: March 22, 2018).

Rodriguez-Ubinas, E., Montero, C., Porteros, M., Vega, S., Navarro, I., Castillo-Cagigal, M.,

Matallanas, E. and Gutiérrez, A. (2014). Passive design strategies and performance of Net Energy Plus Houses. Energy and Buildings, 83, 10–22. https://doi.org/10.1016/j.enbuild.2014.03.074. (Accessed: October 21, 2017)

Rohsenow, W.M., Hartnett, J.P. and Ganić, E.N. (1985). Handbook of heat transfer applications, Mechanical engineering. New York: McGraw-Hill.

Rosti, B. and Omidvar, A. (2013). Study of Annual fluctuation of outside air temperature in transient thermal analysis of exterior building walls. Global Journal of Science, Engineering and Technology. 8, pp. 58-56

Ruivo, C.R., Ferreira, P.M. and Vaz, D.C. (2013). On the error of calculation of heat gains through walls by methods using constant decrement factor and time lag values. Energy Build. 60, 252–261. https://doi.org/10.1016/j.enbuild.2013.02.001. (Accessed: October 21, 2017).

Sun, C., Shu, S., Ding, G., Zhang, X. and Hu, X. (2013). Investigation of time lags and decrement factors for different building outside temperatures. Energy Build. 61, 1–7. https://doi.org/10.1016/j.enbuild.2013.02.003 (Accessed: November 15, 2017).

Velraj, R. and Daniel, G. (2014). Passive Solar Heating or Cooling for Residential Building Using PCM, International Journal of Advanced Research in Civil, Structural, Environmental and Infrastructure Engineering. 2(2), pp. 56-54.

Verbeke, S. and Audenaert, A. (2018). Thermal inertia in buildings: A review of impacts across climate and building use. Renew. Sustain. Energy Rev. 82, 2300–2318. https://doi.org/10.1016/j.rser.2017.08.083. (Accessed: December 10, 2017).

APPENDIX A

WEATHER DATA OF KUMASI

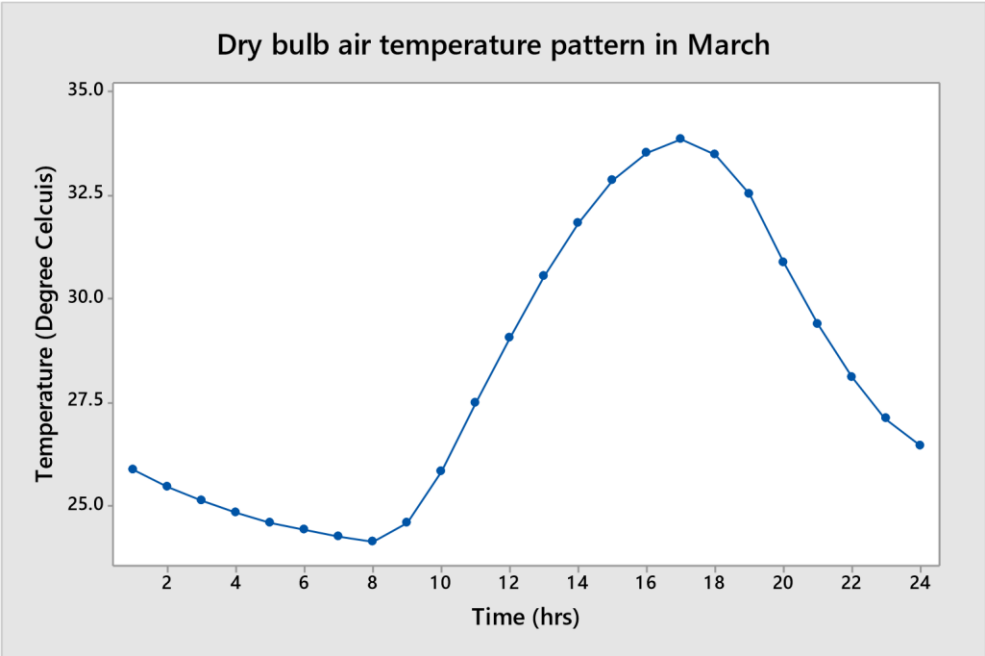

Dry bulb temperature pattern for the month of March

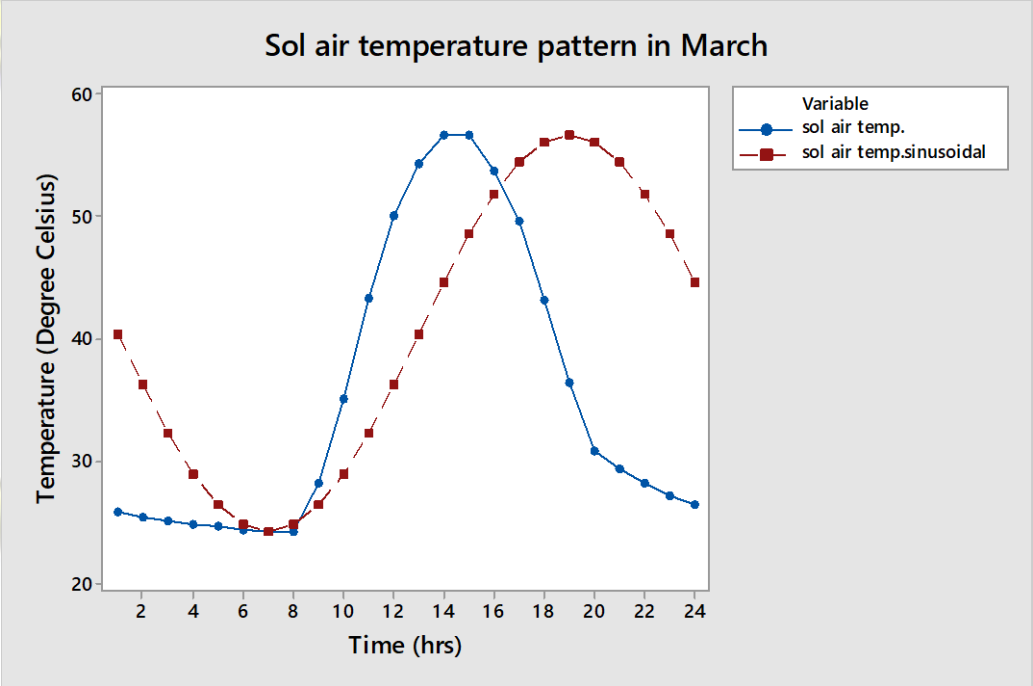

Sol air temperature pattern for vertical surface in March

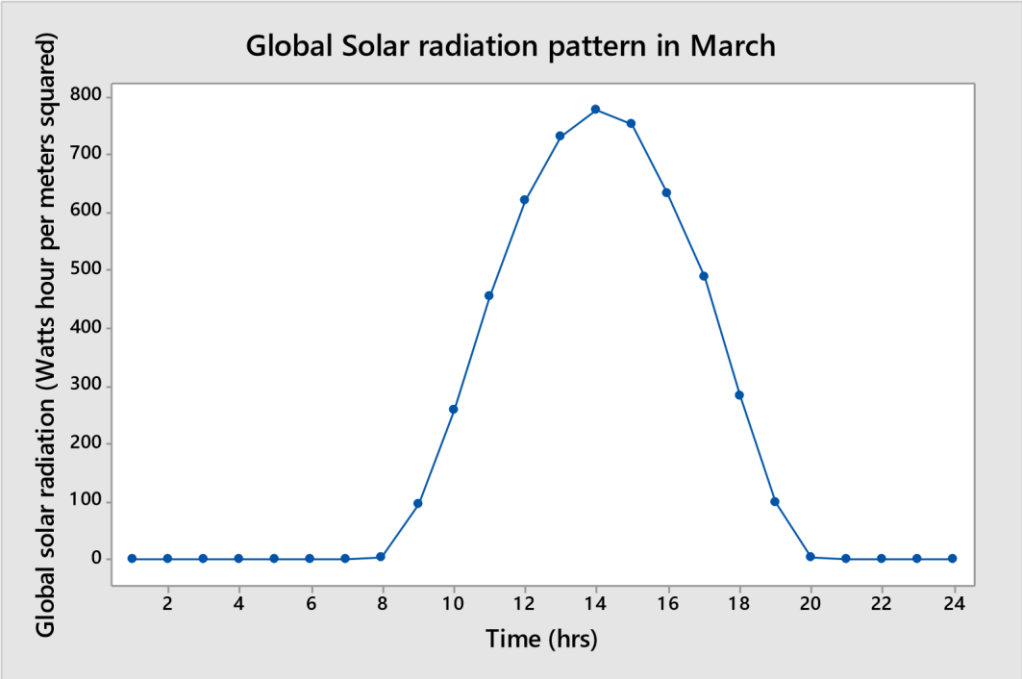

Global solar radiation pattern for the month of March

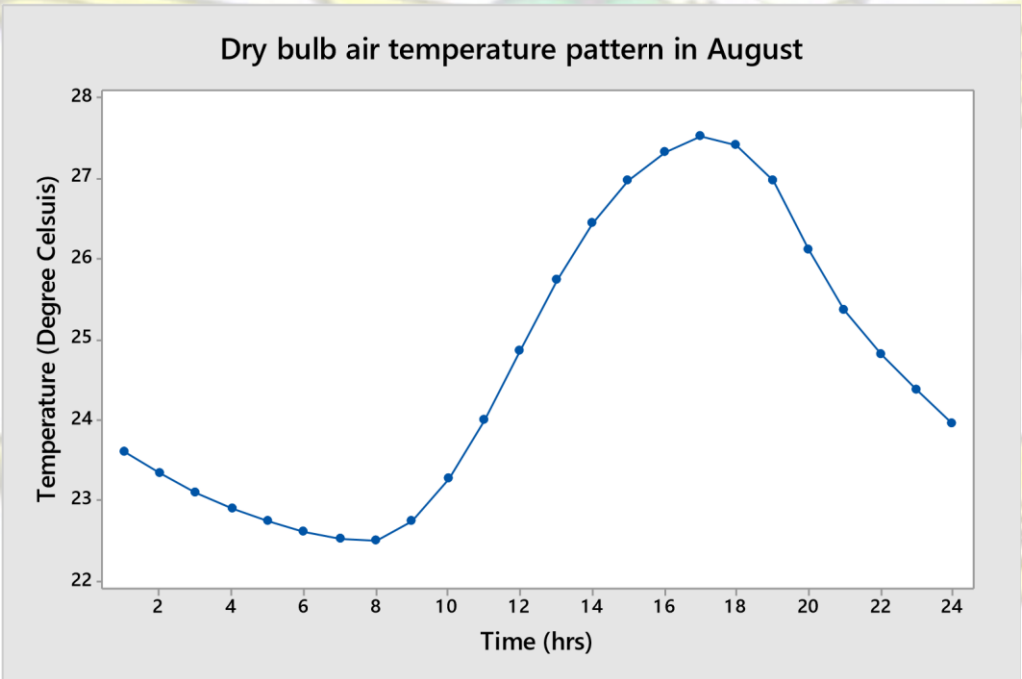

Dry bulb air temperature pattern for the month of August

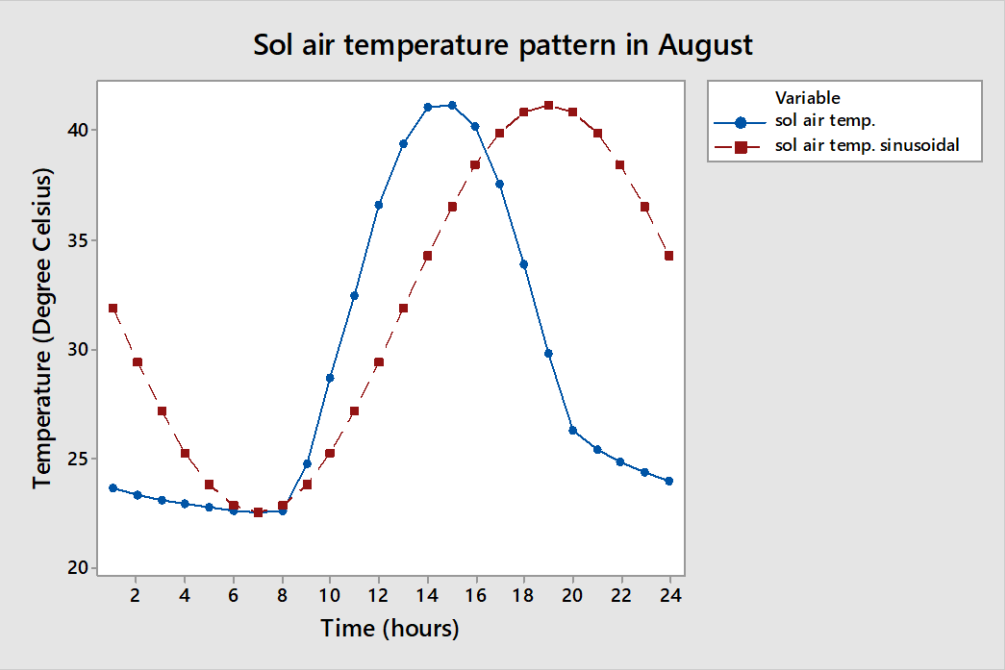

Sol air temperature pattern for vertical surface in August

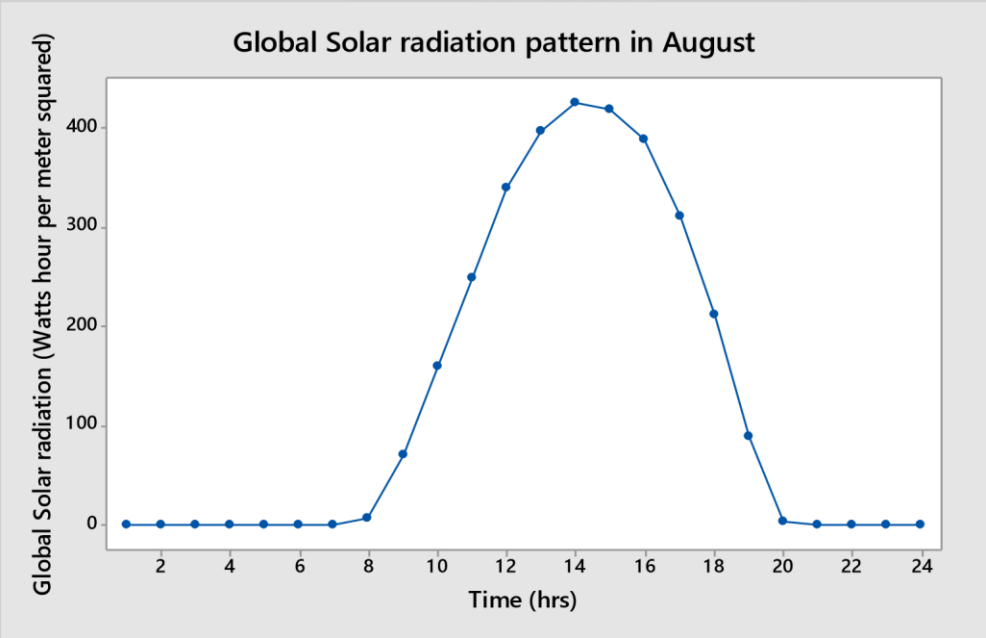

Global solar radiation pattern for the month of August